nature chemistry

ARTICLES

https://doi.org/10.1038/s41557-019-0378-7

Repurposing human kinase inhibitors to create an antibiotic active against drug-resistant *Staphylococcus aureus*, persisters and biofilms

Philipp Le[1,2,19], Elena Kunold[1,2,18,19], Robert Macsics[1,2,19], Katharina Rox[3,4], Megan C. Jennings[5], Ilke Ugur[6], Maria Reinecke[7,8,9], Diego Chaves-Moreno[10], Mathias W. Hackl[1,2], Christian Fetzer[1,2], Franziska A. M. Mandl[1,2], Johannes Lehmann[1,2], Vadim S. Korotkov[1,2], Stephan M. Hacker[11], Bernhard Kuster[7,8,9,12], Iris Antes[6], Dietmar H. Pieper[10], Manfred Rohde[13], William M. Wuest[14,15], Eva Medina[16] and Stephan A. Sieber[1,2,17]*

New drugs are desperately needed to combat methicillin-resistant *Staphylococcus aureus* (MRSA) infections. Here, we report screening commercial kinase inhibitors for antibacterial activity and found the anticancer drug sorafenib as major hit that effectively kills MRSA strains. Varying the key structural features led to the identification of a potent analogue, PK150, that showed antibacterial activity against several pathogenic strains at submicromolar concentrations. Furthermore, this antibiotic eliminated challenging persisters as well as established biofilms. PK150 holds promising therapeutic potential as it did not induce in vitro resistance, and shows oral bioavailability and in vivo efficacy. Analysis of the mode of action using chemical proteomics revealed several targets, which included interference with menaquinone biosynthesis by inhibiting demethylmenaquinone methyltransferase and the stimulation of protein secretion by altering the activity of signal peptidase IB. Reduced endogenous menaquinone levels along with enhanced levels of extracellular proteins of PK150-treated bacteria support this target hypothesis. The associated antibiotic effects, especially the lack of resistance development, probably stem from the compound's polypharmacology.

The current treatment of bacterial infections is challenged by a dramatic increase of multidrug-resistant (MDR) strains[1]. In addition to infections caused by Gram-negative MDR pathogens, Gram-positive pathogens, such as *Staphylococcus aureus*, remain among the top causes of healthcare-associated infections with a high priority in drug development[2]. Especially, methicillin-resistant *S. aureus* (MRSA) has become difficult to treat and causes severe infections[3]. Adding to the challenge is a phenomenon termed persistence, by which a subpopulation of bacteria switches into a dormant state and thereby becomes tolerant towards antibiotics[4]. These persister cells can reinitiate growth after the termination of antibiotic therapy and cause a relapse of the infection and failure of treatment[4]. Moreover, many antibiotics lack the ability to eradicate established biofilms, which are multicellular surface-bound bacterial communities largely composed of bacteria in a dormant persister state.

Although there have been some recent discoveries based on natural products, for example, teixobactin[5], acyldepsipeptides[6] and arylomycins[7], the scope of targets for antibiotics is still extremely narrow. Almost all the marketed antibiotics target cell-wall biosynthesis, membrane integrity, DNA synthesis or protein biosynthesis, all of which have already been counteracted via numerous resistance mechanisms. Given the intricate cellular processes that regulate virulence and viability, a large number of bacterial proteins awaits exploitation as potential antibacterial targets. Research into drugs directed against essential bacterial kinases is still in its infancy[8] and a wealth of eukaryotic kinase inhibitors, originally developed to fight cancer, awaits bacterial testing and putative drug repurposing[9]. Recently, sorafenib (**SFN**), a marketed anticancer drug (Nexavar), and a few derivatives thereof were shown to be effective against MRSA[10,11]. However, at the time it was uncertain if the bacterial target of **SFN** was, indeed, a kinase. Although **SFN**'s core *N*,*N*′-diarylurea motif is also present in other antibacterial compounds, including triclocarban—a *N*,*N*′-diarylurea that was commonly used as an antimicrobial agent in personal care products—the corresponding modes of action are largely unresolved[12,13].

[1]Center for Integrated Protein Science at the Department of Chemistry, Technische Universität München, Garching bei München, Germany. [2]Chair of Organic Chemistry II, Technische Universität München, Garching bei München, Germany. [3]Department of Chemical Biology, Helmholtz Centre for Infection Research, Braunschweig, Germany. [4]German Centre for Infection Research, Partner Site Braunschweig-Hannover, Hannover, Germany. [5]Department of Chemistry, Temple University, Philadelphia, PA, USA. [6]Center for Integrated Protein Science, TUM School of Life Sciences, Technische Universität München, Freising, Germany. [7]Chair of Proteomics and Bioanalytics, Technische Universität München, Freising, Germany. [8]German Cancer Consortium, Partner Site Munich, Munich, Germany. [9]German Cancer Research Center, Heidelberg, Germany. [10]Microbial Interactions and Processes Research Group, Helmholtz Centre for Infection Research, Braunschweig, Germany. [11]Department of Chemistry, Technische Universität München, Garching bei München, Germany. [12]Center for Integrated Protein Science Munich, Garching bei München, Germany. [13]Central Facility for Microscopy, Helmholtz Centre for Infection Research, Braunschweig, Germany. [14]Department of Chemistry, Emory University, Atlanta, GA, USA. [15]Emory Antibiotic Resistance Center, Emory School of Medicine, Atlanta, GA, USA. [16]Infection Immunology Research Group, Helmholtz Centre for Infection Research, Braunschweig, Germany. [17]Helmholtz Institute for Pharmaceutical Research Saarland, Helmholtz Centre for Infection Research, Saarbrücken, Germany. [18]Present address: SciLifeLab, Department of Oncology-Pathology, Karolinska Institutet, Solna, Sweden. [19]These authors contributed equally: Philipp Le, Elena Kunold, Robert Macsics. *e-mail: stephan.sieber@tum.de

a

Organism		MIC (μM) SFN	PK150
Gram-positive			
Staphylococcus aureus	MSSA	3	0.3
	MRSA	3–10	0.3–1
	Clinical isolates	3–10	0.3
	VISA	3	0.3
Enterococcus faecalis	VRE	> 100	3
Enterococcus faecium	VRE	> 100	1
Mycobacterium tuberculosis	H37Rv	25	2
Gram-negative[a]		> 100	> 100

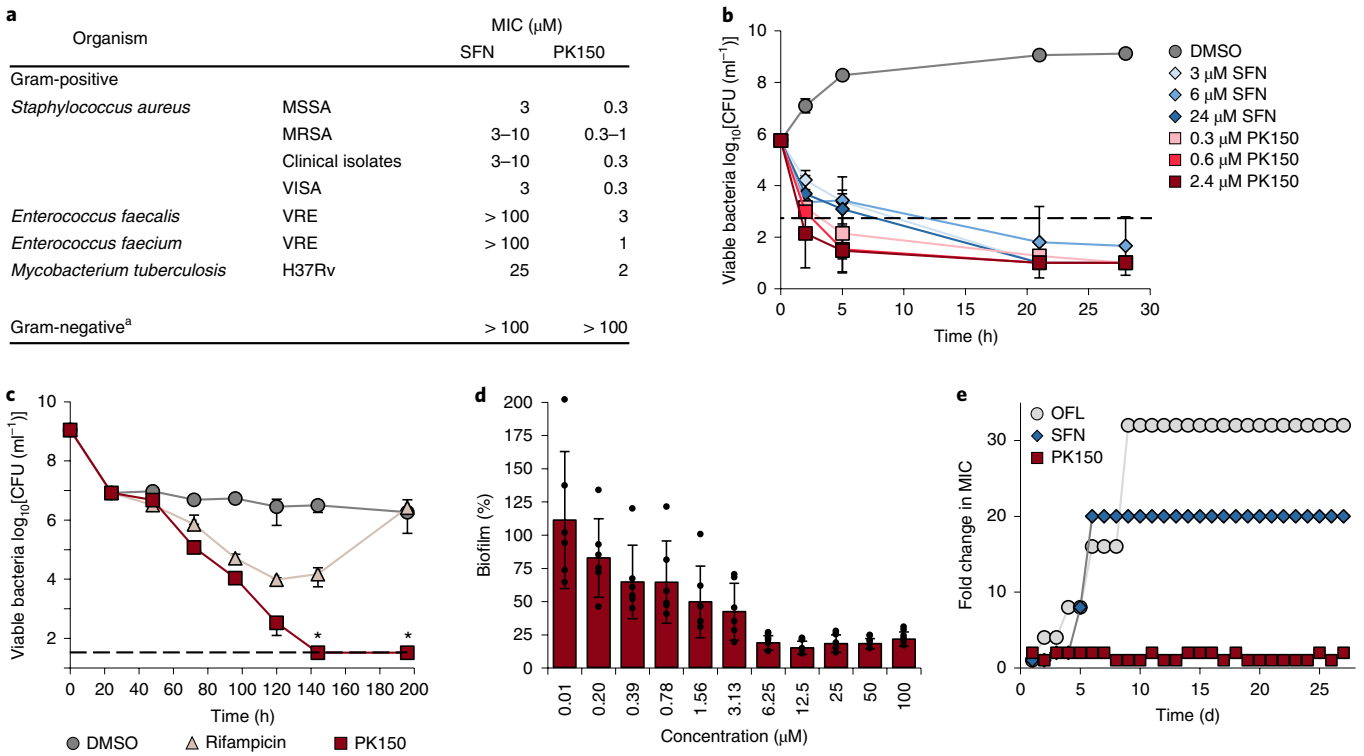

Fig. 1 | Antibacterial properties of SFN and PK150. a, Activity spectra of **SFN** and **PK150** against pathogenic bacteria. Supplementary Data 2 gives details on the specific strains tested. **b**, Time-dependent killing of exponentially growing *S. aureus* NCTC 8325 by different concentrations of **SFN** and **PK150**. The dashed line represents 99.9% of killed bacteria. The data represent average values ± s.d. ($n = 3$ per group). **c**, Persister cell assay. *S. aureus* ATCC 29213 bacteria were incubated with ciprofloxacin (78 μM, 100-fold MIC) for 24 h to isolate persister cells. Bacterial cells were then washed with PBS, resuspended in PBS + 1% (v/v) MH2 medium and treated with rifampicin (0.1 μM, tenfold MIC), **PK150** (2.4 μM, eightfold MIC) or DMSO for 196 h. The data represent average values ± s.d. ($n = 3$ per group); data points marked with an asterisk fall below the limit of detection (33 c.f.u. ml^{-1}, dashed line): no viable bacteria were detected in these cases. **d**, Eradication of *S. aureus* ATCC 29213 biofilm after treatment (24 h) with various concentrations of **PK150**. The data are normalized to DMSO (100% biofilm) and represent average values ± s.d. ($n = 6$ per group). **e**, Resistance development during serial passaging in the presence of sub-MIC concentrations of antimicrobials. Ofloxacin (OFL) served as the positive control. For **SFN**, a 20-fold MIC was the highest concentration tested (solubility limit). The figure is representative for three independent experiments. VISA, vancomycin intermediate *S. aureus*; VRE, vancomycin-resistant enterococci. [a]*A. baumannii*, *E. aerogenes*, *E. cloacae*, *E. coli*, *K. pneumoniae*, *P. aeruginosa*, *S. typhimurium*, *S. enteritides*. The details are given in Supplementary Data 2.

Here we present our findings based on mining small molecule kinase inhibitors for activity against *S. aureus* and confirm **SFN** as one of the most potent hits. Chemical dissection of the **SFN** scaffold by the organic synthesis of 72 analogues resulted in a compound (**PK150**) with tenfold-enhanced anti-MRSA activity, lack of resistance development under laboratory conditions, killing of persisters, elimination of established biofilms and in vivo efficacy in a mouse model. Chemical proteomic studies did not reveal a known kinase as the target, but did show interference with menaquinone biosynthesis and dysregulation of protein secretion as putative target mechanisms.

Results

Antibacterial screen of kinase inhibitors. To access new antibiotic targets with essential functions in *S. aureus* physiology, we screened a library of 232 commercial kinase inhibitors (Supplementary Data 1) for antibacterial activity against the methicillin-sensitive *S. aureus* (MSSA) strain NCTC 8325. Two structurally related compounds, **SFN** and regorafenib, exhibited the lowest minimal inhibitory concentrations (MICs) of 3 μM (1.4 μg ml^{-1}). The antibiotic scope of **SFN** was subsequently evaluated against a panel of Gram-positive and Gram-negative bacteria (Fig. 1a and Supplementary Data 2). Importantly, **SFN** showed activity against antibiotic-sensitive and multidrug-resistant *S. aureus* reference strains as well as ten clinical MRSA isolates, which suggests that the compound acts via a mechanism unrelated to the established resistance pathways. Although no activity was detected against Gram-negative bacteria, inhibition of *Mycobacterium tuberculosis* growth was observed with an MIC of 25 μM (11.6 μg ml^{-1}).

Chemical dissection of SFN results in a compound with enhanced antibiotic potency. To gain a better understanding of the role of the key structural features of **SFN** for its antibiotic properties, we chemically dissected the **SFN** scaffold in an in-depth structure–activity relationship (SAR) study. In total, 72 analogues were synthesized with 40 compounds that bore systematic modifications in all three parts of **SFN**, namely the lateral 4-chloro-3-(trifluoromethyl) phenyl, the central urea and the terminal aryl heteroaryl ether moieties (Table 1). The synthesis of all the analogues followed a modular blueprint as depicted in Supplementary Fig. 1 and their structures are summarized in Supplementary Data 1. Analogues in which the lateral 4-chloro-3-(trifluoromethyl) phenyl moiety was replaced by diverse aliphatic or aromatic groups resulted in inactive molecules. Even minor alterations, such as the removal of substituents (**1-134**, **1-163** and **SFN-C**), abolished the antibiotic activities. In addition, modifications of the central urea motif were restricted (**3-001**). In contrast, the aryl heteroaryl ether motif could be identified as an area for high optimization potential (**2-013**, **3-004**, **3-005**, **3-006**). Importantly, a 2,2-difluoro-1,3-benzodioxole analogue (**PK150**)

Table 1 | Representative derivatives of SFN with their corresponding activities

		MIC (μM)	MIC at 100 μg ml^{-1} MK-4 (μM)	SpsB activity (normalized) at 50 μM
SFN	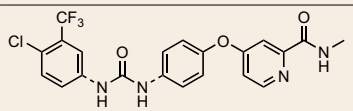	3	20	1.64 ± 0.12
1-134	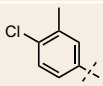	> 100	NA	1.12 ± 0.08
1-163		> 100	NA	1.33 ± 0.20
SFN-C		> 100	NA	1.18 ± 0.16
3-001		10	30	1.58 ± 0.28
2-013	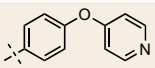	3	7	1.91 ± 0.25
3-004		3	>100	1.49 ± 0.16
3-005	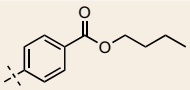	0.6	3-5	2.12 ± 0.25
3-006	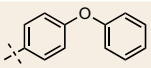	0.5	5	2.10 ± 0.14
PK150	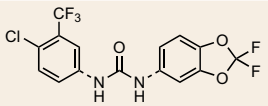	0.3	1-3	2.54 ± 0.39
PK150-C		>100	NA	1.15 ± 0.01
1-159	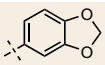	10	>100	1.40 ± 0.01
1-160	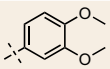	30	50	1.64 ± 0.16
1-164	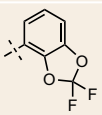	0.5	3	1.42 ± 0.08

Antibacterial activities (MIC against *S. aureus* NCTC 8325), shift of activity in the presence of menaquinone-4 (MK-4) (100 μg ml^{-1}) and SpsB activation potential. The data are derived from three biologically independent experiments performed in triplicate and SpsB activity is given as mean value ± s.d. NA, not applicable: compounds with no intrinsic activity cannot shift MIC by MK-4 and were thus not tested under this condition. A full list of compounds and corresponding activities is given in Supplementary Data 1 and MIC shifts of PK150, SFN and 1-164 at different concentrations of MK-4 are listed in Supplementary Data 2.

exhibited an MIC of 0.3 μM (118 ng ml^{-1}) and thus revealed the highest antibacterial potency among all the compounds. This structural motif appears to be crucial as removal of the fluorine substituents (**1-159**) or opening of the acetal resulting in a dimethoxy analogue (**1-160**) was associated with a significant drop in activity. Changing the regiochemistry by placement of the acetal moiety more proximal to the urea motif (**1-164**) led to a slight decrease in activity. Again, removal of substituents of the 4-chloro-3-(trifluoromethyl) phenyl moiety (**PK150-C**) abolished the antibiotic effect, which highlights the central role of this structural motif.

PK150 was more potent against *S. aureus* NCTC 8325 compared to vancomycin (MIC 1 μM, 1.4 μg ml^{-1}) and linezolid (MIC 3 μM, 1.0 μg ml^{-1}) (Supplementary Data 2). In addition, activity against the panel of MRSA strains was retained and, in contrast to **SFN**, also the killing of vancomycin-resistant enterococci (VRE) was observed (MIC 3 μM, 1.0 μg ml^{-1} (Fig. 1a and Supplementary Data 2)). The compound was active against mycobacteria, including *M. tuberculosis* with an MIC of 2 μM (0.93 μg ml^{-1}), but inactive against all tested Gram-negative bacteria (Fig. 1a and Supplementary Data 2).

PK150 rapidly kills exponentially growing *S. aureus*, largely reduces persisters and established biofilms, and does not induce in vitro resistance. In-depth evaluation of biological properties revealed a bactericidal effect of **PK150** and **SFN** against exponentially

growing MSSA cells (Fig. 1b and Supplementary Fig. 2). In line with this observation, particularly **PK150** disintegrated cells in both a concentration- and time-dependent manner, as shown by the enhanced membrane permeability (Supplementary Fig. 3). Moreover, the amount of persister cells generated from stationary *S. aureus* cultures by ciprofloxacin treatment was effectively reduced in the presence of **PK150**. Unlike rifampicin[14], **PK150** fully eradicated persister cells (Fig. 1c). Persister killing was confirmed in an independent assay format, by which cells at different optical densities were treated with **PK150**, **SFN**, inactive controls and ciprofloxacin or with a combination of these compounds with oxacillin[15]. Again, only **PK150** and **SFN** significantly reduced colony-forming units (c.f.u.) of bacterial cultures by several orders of magnitude throughout all the experiments (Supplementary Fig. 4). In addition, staphylococcal biofilms, largely composed of persisters[16], were effectively eradicated on **PK150** treatment (80% reduction in biofilm after 24 hours of treatment), whereas the antibiotic vancomycin did not significantly affect biofilm integrity (Fig. 1d and Supplementary Fig. 5).

Given these properties, we next tested resistance development against **SFN** and **PK150**. *S. aureus* cells were repeatedly passaged in the presence of different compound concentrations (0.25–4-fold MIC) for 27 days. Although the control antibiotic ofloxacin and **SFN** exhibited a rapid drop in antibacterial activity after a few passages, **PK150** remained active over the complete course of the study (Fig. 1e and Supplementary Fig. 6). Even the addition of the mutagen ethyl methanesulfonate[17] did not trigger resistance development in an agar-plate-based assay format.

Chemical proteomics reveal cellular targets with putative roles in the antibiotic mechanism. Next, we performed target identification studies to understand the mode of action of **SFN** and **PK150**, respectively, by chemical proteomics. The core scaffolds of **SFN** and **PK150** were synthetically equipped with a diazirine photocrosslinker and an alkyne tag (Supplementary Fig. 7), required for affinity-based protein profiling (A*f*BPP) (Fig. 2a)[18,19]. Satisfyingly, the resulting photoprobes **SFN-P** and **3-005-P** (due to the restricted SAR of **PK150** derived from the closest analogue **3-005**) exhibited only a slight increase in MIC of about threefold compared to **SFN** and **PK150**, respectively (Supplementary Data 1). **SFN-P** was used to establish the optimal labelling conditions: intact *S. aureus* cells were incubated with the photoprobe, then irradiated with ultraviolet light to form a covalent linkage with the target protein, lysed and labelled proteins clicked to a rhodamine–biotin azide. Gel-based analysis revealed an optimal concentration of 10–50 µM in both the soluble and insoluble fraction (Fig. 2b and Supplementary Fig. 8). To unravel the identity of the targeted proteins, we performed a quantitative gel-free A*f*BPP analysis by conjugation to rhodamine–biotin azide, enrichment on avidin beads and mass spectrometric (liquid chromatography–tandem mass spectrometry (LC–MS/MS)) analysis (Fig. 2c). To exclude unspecific binding events, three control experiments were performed: (1) incubation with dimethylsulfoxide (DMSO) to account for unspecific avidin binding, (2) competitive labelling in the presence of an excess of **SFN** to confirm that **SFN-P** and **SFN** address the same binding site and (3) comparison to a small portfolio of minimal photocrosslinker probes (**DA-1**, **DA-2** or **DA-3**)[20] to determine the background binding. Tryptic peptides of each experiment were labelled by stable dimethyl isotopes[21] and isotope ratios of the detected peptides were statistically evaluated (Student's *t*-test) for enrichment by the photoprobe, competition with parent **SFN** and background photocrosslinker binding (Fig. 2c,d,g, Supplementary Figs. 9 and 10 and Supplementary Data 3).

Only one protein, signal peptidase IB (SpsB, Q2FZT7), an essential membrane serine endopeptidase involved in the *S. aureus* protein secretion (Sec) pathway[22], consistently exhibited high enrichment ratios ($\log_2$-fold > 3) and confidences ($P < 0.01$) in probe labelling and competition studies and at least an eightfold-less enrichment in background photocrosslinking (red dots in Fig. 2c,d and Supplementary Figs. 9 and 10).

We continued target deconvolution with **PK150** derived **3-005-P** via quantitative, gel-free and label-free A*f*BPP analysis[23] (Fig. 2e,f). These studies revealed only minor alterations in the specificity profile compared to labelling with **SFN-P**. Most importantly, demethylmenaquinone methyltransferase (MenG) pertained as one of the strongest hits that was less enriched with **SFN-P** (Fig. 2f,g, purple dot). MenG catalyses the final step in the biosynthesis of menaquinone, a vitamin crucial for electron transport during bacterial respiration and energy metabolism[24,25].

For proteins that show high enrichment ratios in A*f*BPP experiments with **SFN-P** (blue and grey dots in Fig. 2c,d,g and Supplementary Fig. 9) and/or with **3-005-P** (Fig. 2f,g), MIC shifts of the corresponding transposon mutants (Nebraska transposon mutant library)[26] were determined on treatment with **SFN** and **PK150**, respectively (Supplementary Data 2). Only a mutant in the gene that encoded the lytic regulatory protein (Q2FWA8), a transmembrane protein of unknown function, revealed a slightly decreased susceptibility towards **SFN** and **PK150** (3.3-fold), which indicates a contribution to the overall antibiotic mechanism (Supplementary Data 2). No transposons were available for essential SpsB and MenG. In the case of SpsB, a direct knockout is not available due to its essential function. However, a deletion strain that bears a resistance-induced ABC transporter that bypasses peptidase-mediated secretion is viable, albeit with impaired fitness[27]. In this strain, no MIC shift occurred on **SFN** and **PK150** treatment, respectively, which reinforces that other target(s) may additionally contribute to the overall mechanism.

PK150 lowers menaquinone levels and stimulates SpsB activity. To evaluate whether **SFN** and **PK150** interfere with menaquinone biosynthesis, endogenous levels were determined in viable *S. aureus* cells treated with the compounds. Lysis, menaquinone extraction and quantification by LC–MS indeed revealed a reduction on treatment (Fig. 3a). Moreover, the addition of exogenous menaquinone rescued compound-treated *S. aureus* cells and rendered them less susceptible to **SFN** and **PK150** (Table 1). The MIC shift was dependent on menaquinone concentration and also observed with a variety of bioactive compounds from our diphenyl urea compound library (Table 1 and Supplementary Data 2). As we cannot exclude the contribution of other interfering effects, such as aggregation between menaquinone and the compounds, we independently validated these results by measuring the inhibition of MenG directly. A radioactive enzymatic assay that allows a sensitive readout of the methylation process catalysed by MenG[28] was used to monitor the cellular fate of the radiolabelled methyl group of cofactor *S*-adenosyl-L-methionine ([^{3}H]SAM). Cellular lysate of *S. aureus* NCTC 8325 overexpressing MenG was shown to incorporate significantly less radioactive tritium from [^{3}H]SAM into menaquinone in the presence of **PK150** compared to a DMSO-treated sample (Fig. 3b). In addition, methylation of the non-naturally occurring demethylmenaquinone-2 (DMK-2) by lysates of MenG-overexpressing and wild-type *S. aureus* NCTC 8325 cells was analysed by quantitative LC–MS measurements. Menaquinone-2 (MK-2) synthesis was enhanced in MenG-overexpressing cells and again significantly inhibited by **PK150** (Fig. 3c,d). Overall, similar results were also observed with **1-164**, a regioisomer of **PK150** (Fig. 3a,b,d), whereas **SFN** caused a weaker inhibition in these assays, similar to that observed with the structurally related, but antibiotically inactive **SFN-C** and **PK150-C** (Fig. 3d). Furthermore, as menaquinone deficiency is likely to influence membrane charge distribution, we measured the membrane potential of *S. aureus* cells treated with **PK150** or with **SFN** and found both compounds to reduce the potential (Supplementary Fig. 11 and Supplementary Discussion give the details).

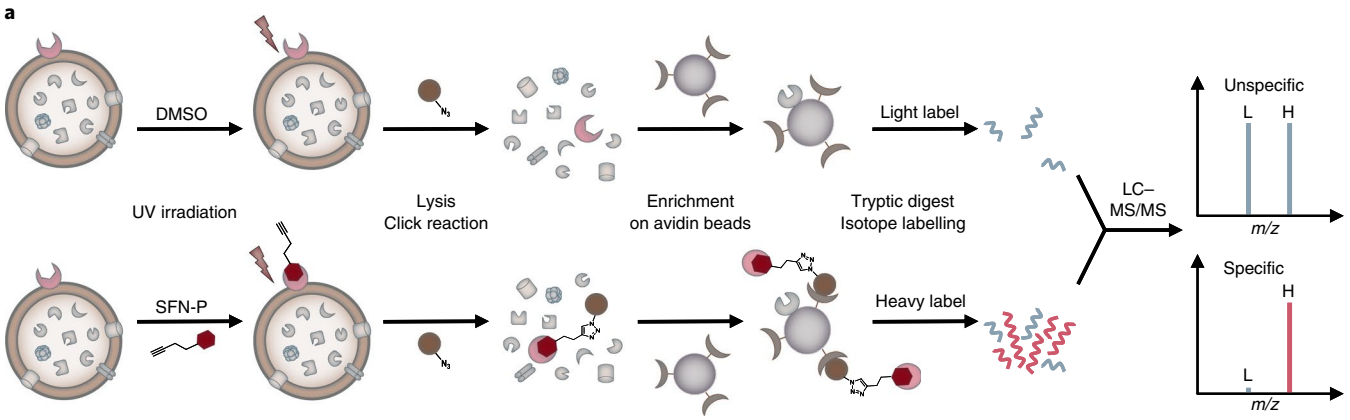

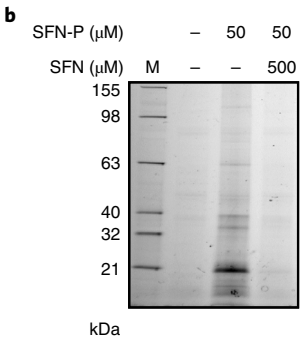

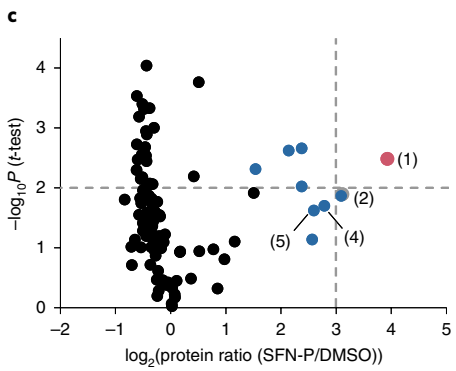

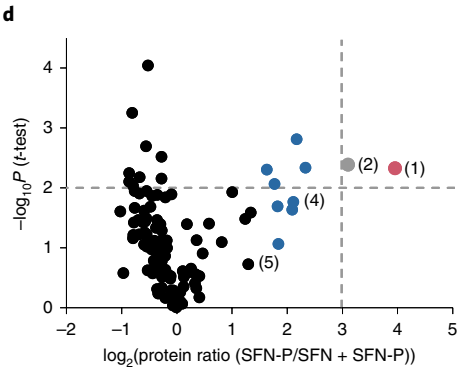

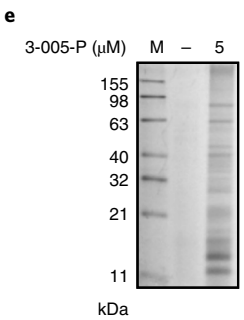

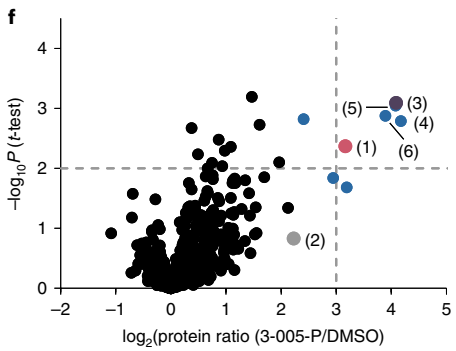

g

	Abbreviation	Protein name	UniProt ID
(1)	SpsB	Signal peptidase IB	Q2FZT7
(2)	Lyt	Lytic regulatory protein	Q2FWA8
(3)	MenG	Menaquinone biosynthesis methyltransferase	Q2FYG5
(4)	–	Uncharacterized protein	Q2FVZ5
(5)	–	Uncharacterized protein	Q2G193
(6)	–	Uncharacterized protein	Q2G117

Fig. 2 | Target identification by chemical proteomic profiling in *S. aureus*. a, Schematic experimental workflow for target identification by A*f*BPP. Intact cells were treated with a probe or DMSO (as control), ultraviolet (UV) irradiated, lysed and the labelled proteins clicked to rhodamine–biotin azide (note that the probe is capable of binding extracellular as well as intracellular targets). After enrichment on avidin beads, the proteins were enzymatically digested and finally appended to either light (L) or heavy (H) isotopes via dimethyl labelling. Ratios of H/L peptides were determined via subsequent LC–MS/MS measurements. **b**, Fluorescence SDS–PAGE showing labelling of *S. aureus* NCTC 8325 cells with **SFN-P** (50 μM) and competition with a tenfold excess of **SFN** (0.5 mM) before enrichment on avidin beads. The gel is representative for three biologically independent experiments. **c**,**d**, A*f*BPP experiments using **SFN-P**. Volcano plots show a $\log_2$-fold enrichment of proteins in the soluble fraction after treatment of *S. aureus* NCTC 8325 cells with **SFN-P** (50 μM) compared with DMSO (**c**) or to pretreatment with the competitor **SFN** (500 μM) (**d**). The vertical and horizontal dashed lines represent a $\log_2$-fold enrichment ratio of 3 and a $-\log_{10}P$ value of 2 (two-sided one sample *t*-test over normalized protein ratios), respectively. The Benjamini–Hochberg significance threshold is at a $-\log_{10}P$ value of 1.7 for labelling and 3.3 for competition studies, respectively (false discovery rate of 0.05). The red dot represents the essential protein SpsB. Blue dots represent proteins for which respective transposon mutants were tested for MIC shifts of **SFN** and **PK150** in comparison to the MIC in the wild type; no MIC shifts were observed. The grey dot represents the lytic regulatory protein whose transposon mutant has shown a shift in MIC to 10 μM (**SFN**) and 0.3–1 μM (**PK150**); Supplementary Data 2 gives the transposon mutants tested. The data represent average values; $n = 3$ biologically independent experiments performed in triplicate. **e**, Fluorescence SDS-PAGE showing labelling of *S. aureus* NCTC 8325 cells with **3-005-P** (5 μM) after enrichment on avidin beads. The gel is representative for three biologically independent experiments. **f**, A*f*BPP experiment using **3-005-P**. The volcano plot shows a $\log_2$-fold enrichment of proteins after treatment of *S. aureus* NCTC 8325 cells with **3-005-P** (5 μM) compared with DMSO in a label-free proteomic profiling experiment. Soluble and insoluble proteins were not separated and measured together. Dashed lines represent a $\log_2$-fold enrichment ratio of 3 and a $-\log_{10}P$ value of 2 (two-sided two-sample *t*-test over LFQ intensities), respectively. Blue dots represent proteins whose respective transposon mutants were tested and did not exhibit an MIC shift against **SFN** and **PK150**. The grey, red and purple dots denote the lytic regulatory protein, SpsB and MenG, respectively. The data represent average values from three biologically independent experiments performed in triplicate. **g**, Table that allocates the six major protein hits from the A*f*BPP experiments with both photoprobes **SFN-P** and **3-005-P** to the volcano plots in **c**, **d**, **f** and Supplementary Fig. 9.

We next tested if **SFN** and **PK150** bind to SpsB and if this binding affects peptidase activity. SpsB was cloned, overexpressed in *Escherichia coli* and labelled by **SFN-P** in situ (Fig. 3e and Supplementary Fig. 12). Pre-incubation with **SFN** and **PK150** significantly reduced the signal, which validates target binding of the parent compound. No competition was observed with **PK150-C**. **SFN-C** still reduced the signal, which indicates a residual binding affinity (Supplementary Fig. 12).

Utilizing a fluorescence resonance energy transfer (FRET)-based assay (Fig. 3f)[29,30], *E. coli* membranes induced for SpsB expression (Fig. 3g) and *S. aureus* membranes that contained native SpsB (Supplementary Fig. 13) were incubated with a fluorogenic SpsB substrate. Substrate turnover was low in *E. coli* membranes that lacked SpsB expression. Surprisingly, the addition of **SFN** resulted in a significant stimulation of enzymatic substrate hydrolysis by 27% at 10 μM and up to 32% at 50–100 μM compared to the DMSO control in *E. coli* membranes (Fig. 3g). Similar results were obtained with *S. aureus* membranes that contained endogenous SpsB (Supplementary Fig. 13). Interestingly, **PK150** enhanced the substrate turnover even more strongly with a 1.7-fold elevated activity compared to **SFN** in induced *E. coli* and native *S. aureus* membranes (which corresponds to a maximum increase by 2.3–2.9-fold over the base activity (Fig. 3g and Supplementary Fig. 13)). Very limited or no activation was achieved with the structurally related, but antibiotically inactive, analogues **SFN-C** and **PK150-C**. Activation of SpsB was seen with several antibiotically active members of the library (Table 1, Fig. 4a, Supplementary Fig. 14 and Supplementary Data 1). An elevated turnover comparable to that of the membrane assays was also observed with the enzyme purified from the cytosolic fraction (Supplementary Fig. 13). Further results on the validation of this assay and the activation of SpsB are given in the Supplementary Discussion and Supplementary Figs. 15–18.

We next investigated the molecular basis for SpsB activation by docking together with molecular dynamics simulations[31]. The refined docking pose with the best binding free energy suggested that **PK150** was located adjacent to the active site with an average distance of 12 Å between its centre and the Cα atom of the active site residues S36 and K77 (Supplementary Fig. 19). Here the CF_3 alkyl unit of **PK150** is predicted to interact predominantly with four non-polar amino acids, namely L41, V47, V64 and V170, which form a hydrophobic surface patch to yield strong hydrophobic interactions (Supplementary Fig. 19). In addition, the urea group of **PK150** forms crucial hydrogen bonds with D147 (Supplementary Fig. 19). Supported by SAR data (Fig. 4a), these two invariant structural moieties seem to be hallmarks of **PK150** binding into the SpsB groove.

Molecular dynamics simulations were applied to elucidate the origin of activation. Interestingly, **PK150** binding initiates changes in the secondary structure, which include both destabilization and stabilization (Supplementary Fig. 19), and thereby rigidifies the peptide substrate binding areas, the loop region containing the active site Ser and the residues in direct proximity of the active site dyad (brown, grey and pink boxes in Supplementary Fig. 19).

SFN and PK150 dysregulate protein secretion and induce autolysis. Although the inhibition of SpsB with arylomycin, which is believed to cause cell death by accumulation of unprocessed proteins, has been studied by proteomic analysis of the bacterial secretome[32–34], little is known about the underlying stimulating effects. To understand how activation of SpsB affects the secretome, we analysed extracellular proteins in the presence of **SFN** and **PK150** as well as in the presence of inactive **SFN-C** and **PK150-C** (Table 2, Fig. 4b and Supplementary Fig. 20). Secretomes of treated cells were precipitated, digested with trypsin and quantified by label-free mass spectrometry[23]. Statistical analysis of the antibiotic-treated cells revealed elevated levels of SpsB-processed proteins in the secretome compared with those in DMSO- and inactive control compound-treated cells (Fig. 4b, Supplementary Fig. 20 and Supplementary Data 4)[35].

Proteins bound to the membrane surface of **SFN**- and **PK150**-treated bacteria were shaved by tryptic digest and analysed via

Fig. 3 | Validation of cellular targets with putative roles in the antibiotic mechanism. a, Metabolic profiling of endogenous menaquinone levels in *S. aureus* NCTC 8325 cells on compound treatment. Bacteria were treated with subinhibitory concentrations (0.1-fold to 0.5-fold of the respective MIC) of **PK150**, **1-164**, **SFN** or vancomycin (VANCO). Menaquinone-8 (MK-8) was extracted by solid phase extraction and quantified by LC–MS, using single-ion monitoring (SIM) and menaquinone-9 as the internal standard. MK-8 levels are normalized to DMSO-treated samples. Each colour represents an individual independent extraction experiment, where differently shaped symbols (circles, triangles and diamonds) indicate independent biological samples. Error bars denote mean values ± s.d. ($n = 7$ for **PK150** and **SFN**, $n = 4$ for **1-164** and $n = 6$ for VANCO). **b**, Radioactive enzymatic assay monitoring the transfer of the radiolabelled methyl group of [^{3}H]SAM to DMK-2. A cellular lysate of *S. aureus* pRMC2-MenG (20 mg ml^{-1} total protein concentration) was incubated with [^{3}H]SAM, DMK-2 and different concentrations of **PK150**, **1-164** or **SFN**. After an 80 min incubation period, menaquinone was extracted with hexane/2-propanol 3:2 and the radioactivity in the organic phase was measured by liquid scintillation counting. 'No substrate' indicates the background activity in the absence of DMK-2. Values represent mean ± s.d. of independent replicates ($n = 5$ for DMSO, 10 μM conditions and no substrate; $n = 3$ for 2 μM and 20 μM conditions) and are normalized to the DMSO-treated control. **c**,**d**, Enzymatic assay monitoring the methylation of DMK-2 by LC–MS. The cellular lysate of either *S. aureus* pRMC2-MenG or *S. aureus* NCTC 8325 (20 mg ml^{-1} total protein concentration) was treated with [^{3}H]SAM, DMK-2 and different concentrations of **PK150**, **1-164** and **SFN** or the respective controls (**SFN-C** and **PK150-C**). After an 80 min incubation period, the menaquinones were extracted by solid-phase extraction and the production of MK-2 was quantified by LC–MS, using SIM with MK-4 as the internal standard. The MenG-overexpressing strain pRMC2-MenG (MenG(+)) produces more MK-2 compared with the wild-type NCTC 8325 (WT), as indicated by the total area under the curve (AUC) ± s.d., $n = 3$, of the SIM peak of MK-2 (**c**). MK-2 quantities were normalized to the respective DMSO-treated samples and represent the averaged values ± s.d. from three independent experiments (**d**). **e**, Labelling of recombinant SpsB. The fluorescence gel shows the labelling patterns after pretreatment of *E. coli* BL21(DE3)pLysS cells that harbour pET-55-DEST-SpsB (either induced (+) or not induced (−) for the expression of SpsB (molecular mass 24,951 Da)) with DMSO (control), **SFN** or **PK150** (500 μM; competition) and subsequent incubation with **SFN-P** (50 μM). Two lanes that represent purified SpsB are omitted for clarity and are depicted in Supplementary Fig. 12 together with the corresponding Coomassie stain. The gel is representative for two independent experiments. **f**, Schematic representation of the FRET assay to measure the activity of membrane-bound SpsB via the cleavage of a FRET peptide substrate. The FRET peptide substrate is based on the signal peptide sequence of the *S. epidermidis* SceD preprotein modified with the fluorescent donor 5-((2-aminoethyl)amino)-1-naphthalenesulfonic acid (EDANS) and the quenching acceptor 4-((4-(dimethylamino)phenyl)azo)benzoic acid (DABCYL). **g**, **SFN**- and **PK150**-induced concentration-dependent cleavage of the FRET substrate by membrane-bound SpsB (50 μg ml^{-1} total membrane protein concentration). The substrate cleavage rates are normalized to DMSO-treated samples from the induced membranes. Membranes were extracted from *E. coli* BL21(DE3)pLysS cells that harbour pET-55-DEST-SpsB (either induced (+) or not induced (−) for the expression of SpsB). The bars highlight the SpsB activity at a 10 μM compound concentration relative to DMSO. All the data represent mean values ± s.d. of averaged triplicates of $n = 3$ biologically independent experiments per group; NS, not significant, $P = 0.2023$; $^*P = 0.0249$, $^{***}P = 0.00045$, $^{****}P = 1.76 \times 10^{-5}$ (two-sided unpaired parametric *t*-test) for compound- versus DMSO-treated groups.

LC–MS/MS. In line with the proposed mechanism of activation, the abundance of membrane-residing SpsB substrate proteins was reduced in **SFN**- and **PK150**-treated cells compared to that in treatments with DMSO or inactive **SFN-C** and **PK150-C**, respectively (Fig. 4c and Supplementary Fig. 20).

Bioinformatic analysis of proteins with enhanced secretion on SpsB stimulation revealed that peptidoglycan hydrolase (PGH)-domain-containing proteins (autolysins (Supplementary Data 4)) were significantly overrepresented in the secretomes of **PK150**- and **SFN**-treated cells (unlike in the inactive control samples (Table 2 and Supplementary Table 1)). These autolysins break down peptidoglycan and facilitate cell division, which is controlled by peptidoglycan-bound teichoic acid molecules. In fact, previous studies with inducible autolysin expression vectors revealed that minor imbalances of secreted autolysins result in dysregulation of cell-wall biosynthesis and consequently induce rapid cell death[36,37]. The extracellular accumulation of PGH-domain-containing proteins on antibiotic treatment as seen here (Supplementary Data 4) could probably provoke such imbalances and result in the induction of autolysis. Interestingly, analysis of autolysin activity via zymography of *S. aureus* cells treated with **SFN** and **PK150** revealed a characteristic induction of several hydrolytic enzymes in the higher molecular mass range (Supplementary Fig. 21). These bands were also observed with penicillin G. In contrast, no such induction occurred on treatment with inactive **SFN-C**, **PK150-C** and DMSO. Taken together, these results indicate that **SFN** and **PK150** probably kill *S. aureus* by altering protein secretion, which includes disbalances in secreted autolysin levels.

To obtain additional insights into the antibiotic mechanism, we performed field emission scanning electron microscopy

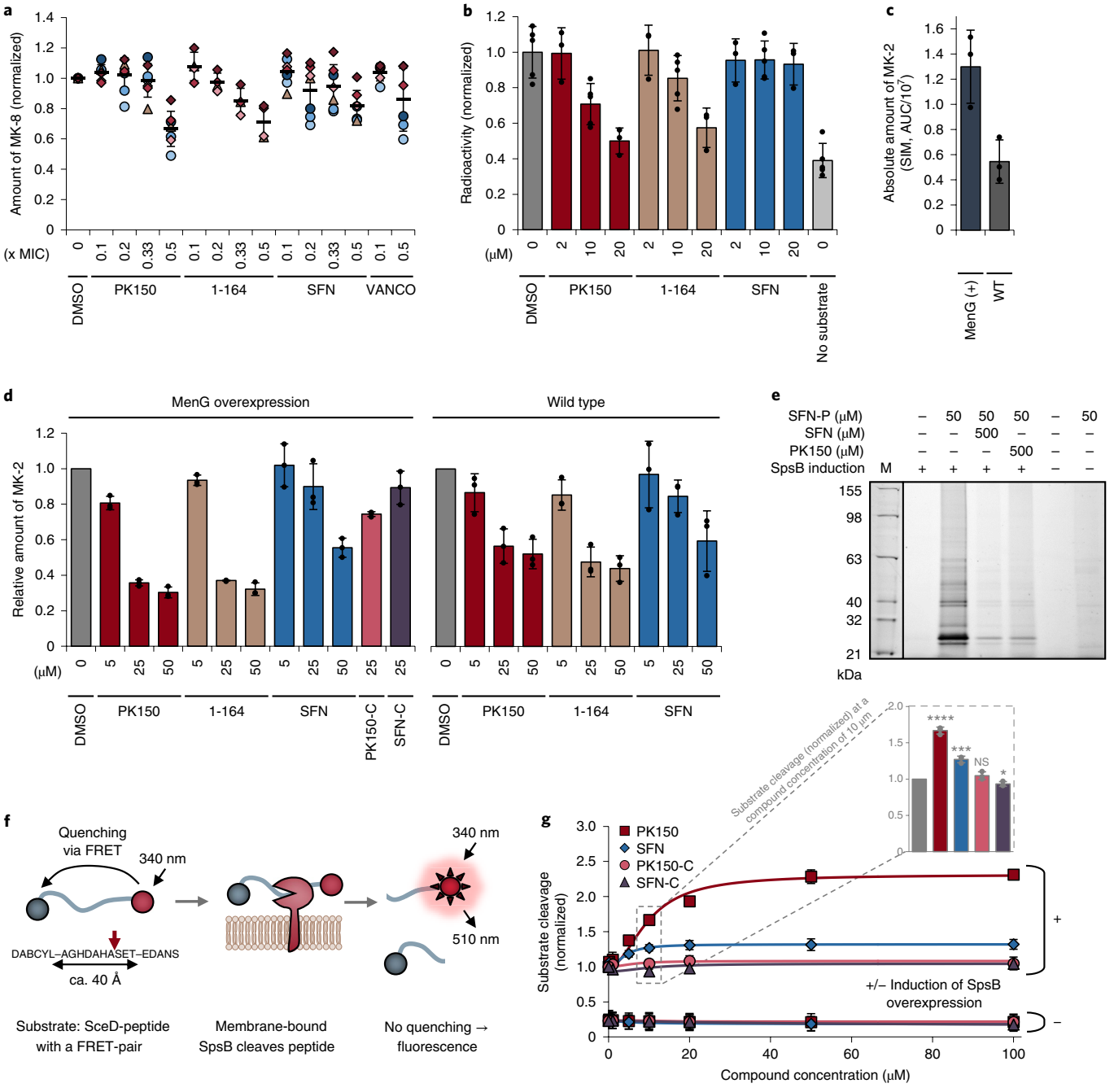

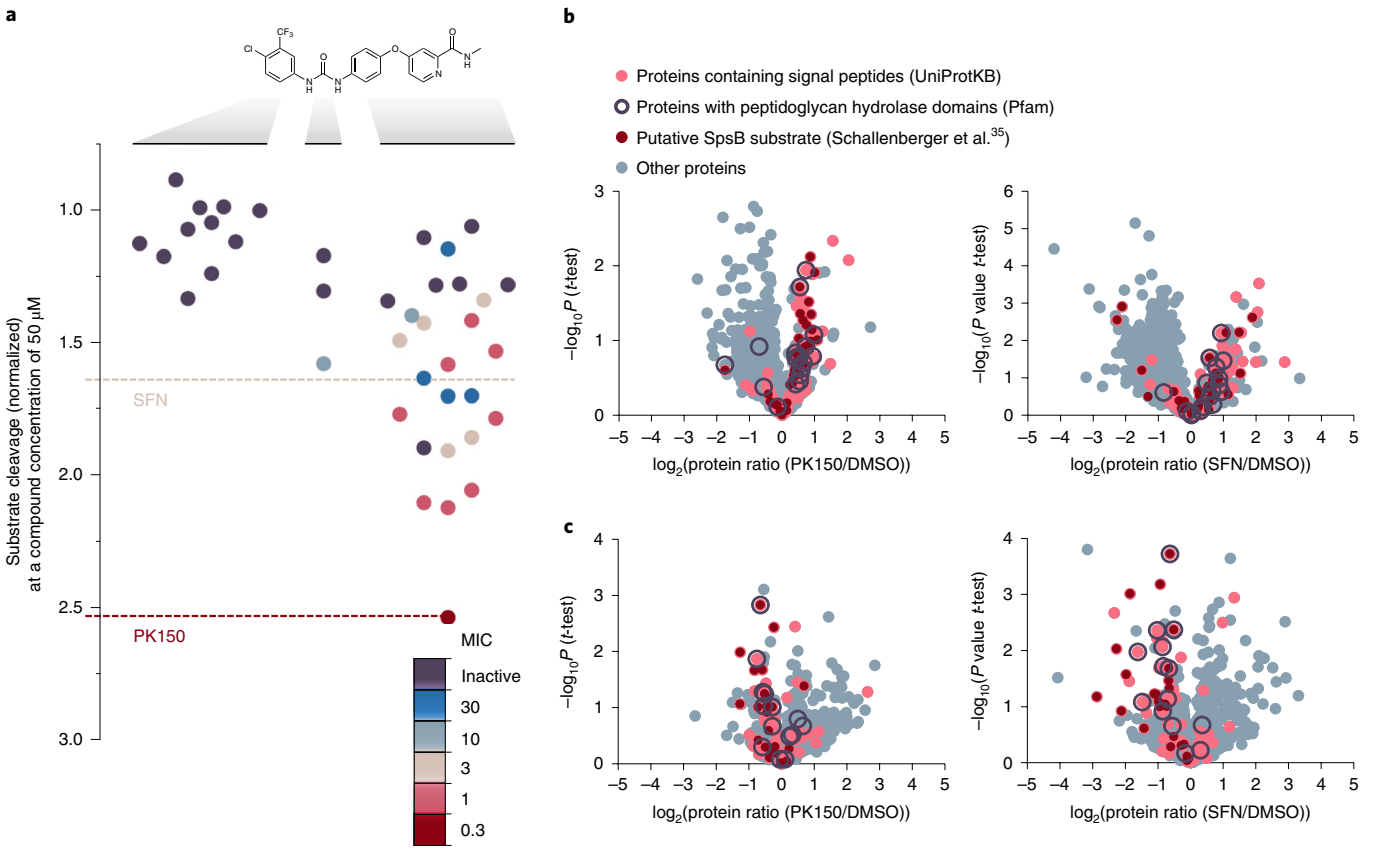

Fig. 4 | SAR study of SFN and mode of action analysis by chemical proteomics. a, The SAR study with 40 analogues of **SFN** highlights the role of various structural key elements for the activation of SpsB (box plot) as well as antibacterial activity (colour code). Antibacterial activity was tested against *S. aureus* NCTC 8325; MIC values are represented according to the introduced colour code. SpsB activity was determined by a FRET-based activity assay using *S. aureus* NCTC 8325 membranes that contained endogenous SpsB (0.2 mg ml^{-1} total membrane protein concentration, 50 µM compound concentration). The substrate cleavage rates are normalized to DMSO-treated samples. A full list of compounds, structures and activities is given in Supplementary Data 1. **b**, Secretome analysis. The volcano plots show a $\log_2$-fold change of protein levels in the secretome after treatment of *S. aureus* NCTC 8325 cells with **PK150** (0.15 µM, 0.5-fold MIC) (left) or **SFN** (1.5 µM, 0.5-fold MIC) (right) compared with DMSO treatment. The dark red dots represent proteins whose secretion was found to be inhibited by Arylomycin C16 (experimentally proposed SpsB substrates)[35]. The light red dots represent proteins that are predicted to have an SpsB signal peptide motif (according to UniProtKB as annotated by SignalP)[61]. The purple circles represent proteins that contain PGH domains (Pfam annotations)[55]. The data represent averaged values and the *P* values were calculated using a two-sided two-sample *t*-test, $n = 4$ independent experiments per group. **c**, Surfaceome analysis. The volcano plots show the $\log_2$-fold change of protein levels in the surfaceome after treatment of *S. aureus* NCTC 8325 cells with **PK150** or **SFN** (0.5-fold MIC) compared with DMSO. Colour coding is equivalent to that in **b**. The data represent averaged values and the *P* values were calculated using a two-sided two-sample *t*-test, $n = 4$ independent experiments per group.

(FESEM) and transmission electron microscopy (TEM) examination. Whereas FESEM micrographs of bacteria treated with **PK150-C** (Fig. 5a) or DMSO (Supplementary Fig. 22) showed no cellular abnormalities, **PK150** incubation induced extracellular vesicle formation at the septum of dividing cells (Fig. 5b and Supplementary Fig. 22). Moreover, lysis and full degradation of the cells were observed only in bacteria treated with **PK150** (Fig. 5c,d and Supplementary Fig. 22). A closer inspection of the membranes in ultrathin sections of **PK150**-treated *S. aureus* via TEM showed that the extracellular vesicle formation was initiated by protrusions of cytoplasmic membrane through gaps in the cell wall, which was absent in both controls (Fig. 5e,f and Supplementary Fig. 22). Two different cytoplasmic cargos that consist of intracellular material (Fig. 5e) or DNA (Supplementary Fig. 22) were detected in extracellular vesicles. Moreover, cellular disintegration by **PK150** could be visualized at various stages (Supplementary Fig. 22). The lack of peptidoglycan at the sites of vesicle formation (Fig. 5f) suggests active cell-wall degradation and a burst of the extruded cytoplasmic membrane as the mode of action. Given the known location of autolysins at the septum of dividing cells[38], their dysregulation at these sites supports the antibiotic mechanism of **PK150**.

Autolysin secretion and SpsB activity are decreased in SFN-resistant strains. To elucidate further the overall mechanism, we selected **SFN**-resistant *S. aureus* isolates from our resistance development assays (Fig. 1e and Supplementary Fig. 6) and subjected them to whole-genome sequencing. Aside from a few mutations found only in part of the sequenced isolates, all the clones carried frameshift mutations in SAOUHSC_01359 (*mprF*) encoding phosphatidylglycerol lysyltransferase fmtC (Q2G2M2) (Supplementary Table 2 and Supplementary Data 5 give details, which include a list of all mutations). MIC shift assays with the corresponding transposon mutants of all the affected genes did not result in altered sensitivity towards **SFN** compared to the wild type (Supplementary Data 2). We thus assumed a more general mechanism that indirectly influences target activity. To investigate this hypothesis in more detail, we first tested whether resistance provoked changes on the proteome level. No corresponding peptides of fmtC (mprF; Q2G2M2)

Table 2 | Enrichment analysis of PGH domain-containing proteins

Category	PK150/DMSO	SFN/DMSO	Secretome
	Proteins with log_2(protein ratio) >0.5		
Total proteins	83	121	806
'PGH domain and signal predicted/AC16 responder' proteins	10	9	12
Not 'PGH domain and signal predicted/AC16-responder' proteins	73	112	794
Fisher exact *P* value (secretome as background)	4.47×10^{-9}	4.38×10^{-6}	

Pfam annotations[60]: CHAP domain, LysM domain, amidase, transglycolase, glucosaminidase and peptidase M23 domain. A two-sided Fisher's exact test was used among proteins that showed a log_2-fold enrichment >0.5 in the secretome (full measured secretome of $n=806$ total proteins was used as background). Further details in Supplementary Table 1.

were found in our MS measurements (Fig. 6a and Supplementary Data 4), which corresponds well to the results from whole-genome sequencing. Moreover, the downregulation of several PGH domain-containing proteins was observed in the proteome of **SFN**-resistant isolates (Fig. 6a and Supplementary Data 4). This downregulation probably counteracts their elevated extracellular secretion on antibiotic treatment. Interestingly, the transcriptional regulator ArcR (HTH-type transcriptional regulator ArcR; Q2FUY1) and several enzymes of the corresponding arginine deiminase pathway (Fig. 6a and Supplementary Data 4), responsible for ATP production via arginine catabolism under oxygen-limiting conditions[39], were found to be upregulated, which suggests a switch to an alternative energy metabolism of resistant cells.

FmtC is involved in the modification of membrane lipid phosphatidylglycerol with positively charged amino groups (lysine)[40]. It regulates biophysical properties of the membrane and thereby might influence the activity of key enzymes of the cell wall[41,42]. In line with this function, SpsB stimulation by **SFN** in the resistant isolates was diminished, as shown in the FRET-based peptidase assays using membrane fractions from **SFN**-resistant isolates as the source for endogenous SpsB (Fig. 6b). Interestingly, membranes derived from the corresponding transposon mutant of fmtC were still activated by both **SFN** and **PK150**, albeit at a lower level than in the wild type (Fig. 6b). In-depth secretome analysis further revealed no increase in SpsB-dependent protein secretion on **SFN**-treatment in resistant bacteria (Fig. 6c). In particular, levels of PGH domain-containing proteins (Supplementary Data 4) seem to be tightly controlled even after antibiotic treatment. For further findings related to the **SFN**-resistant isolates, please refer to the Supplementary Discussion, Supplementary Data 4, Supplementary Table 3 and Supplementary Fig. 23.

PK150 is orally bioavailable and effective in the treatment of in vivo *S. aureus* infections. Based on its potency and lack of resistance development, we further evaluated the pharmacological profile of **PK150**. First, we utilized the kinobeads technology[43] to evaluate if **PK150** still exhibited kinase affinity, which could contribute to toxic side effects. Lysates of four human cancer cell lines (K-562, Colo 205, SK-N-BE(2) and MV-4-11) were incubated with kinobeads, which captured a vast variety of more than 250 human kinases, in the presence or absence of **SFN** and **PK150**. Mass spectrometry analysis of these competitive affinity pull downs revealed that, in contrast to **SFN**, which was bound to eight human kinases, **PK150** exhibited no affinity to any kinase (Supplementary Data 6 and Supplementary Fig. 24).

The in vitro toxicity of **PK150** was determined by MTT assays against a panel of human and murine cell lines, which revealed

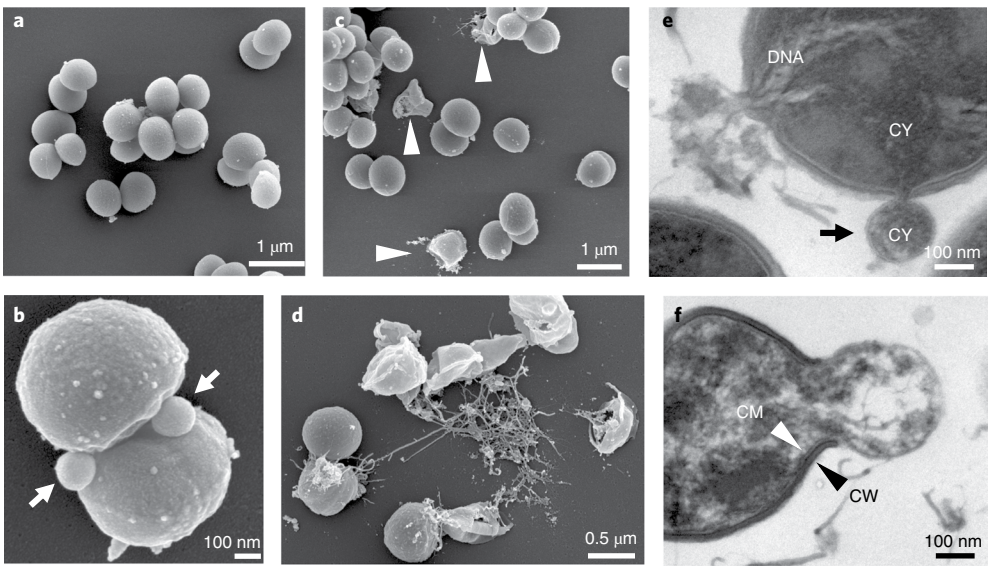

Fig. 5 | FESEM and TEM of *S. aureus* NCTC 8325. a–d, FESEM of *S. aureus* NCTC 8325 treated with the inactive control compound **PK150-C** (2.4 µM) (**a**) or **PK150** (1.2 µM (**b**) or 2.4 µM (**c**,**d**)). Round and smooth shapes indicate healthy cells for the control (**a**) and DMSO-treated (Supplementary Fig. 22) cells, whereas **PK150**-treated cells show deviations in the cell appearance (**b**–**d**). Arrow heads point to damaged *S. aureus* (**c**). **b**,**d**, Two modes of action of **PK150** are visible, namely extracellular vesicle formation with cytoplasmic content, predominantly in the division zone of the bacteria (**b**, arrows), and extrusion of DNA-containing material (**d**). Images are representative for 75 recordings from two independent preparations. **e**,**f**, TEM of *S. aureus* NCTC 8325 treated with **PK150** (2.4 µM). The two modes of action of **PK150** can also be observed in TEM images—the formation of extracellular vesicles (**e**) (the black arrow points towards the cytoplasmic membrane (CM) of the vesicle), which probably burst and release the entire cytoplasmic content to leave cell-wall relicts (**f**). CY, cytoplasm; CW, cell wall. Images are representative for 210 recordings from three independent preparations.

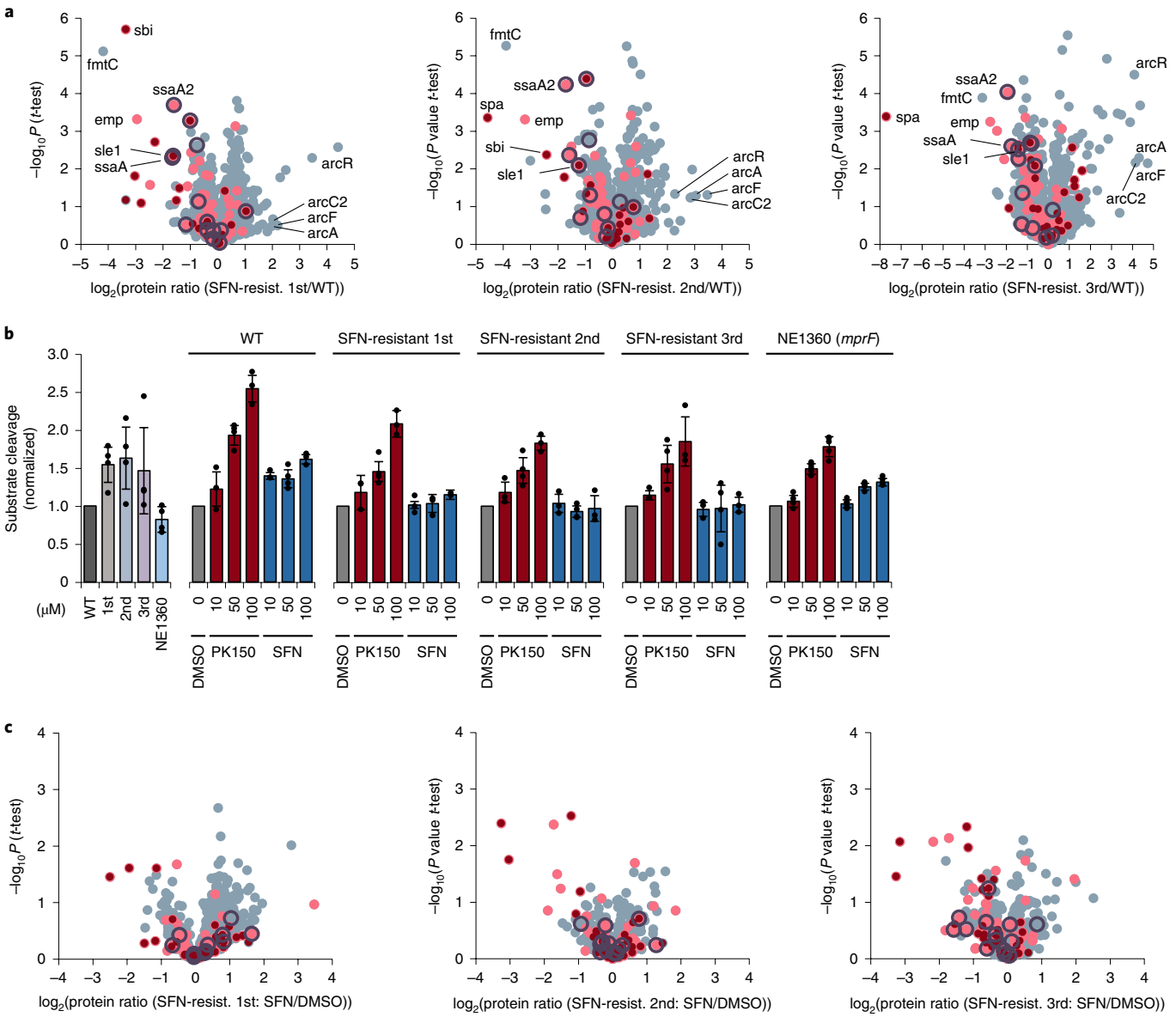

Fig. 6 | In-depth analysis of SFN-resistant *S. aureus* isolates and accompanying consequences for compound-induced SpsB stimulation. a, Proteome analysis of **SFN**-resistant isolates. The volcano plots show a $\log_2$-fold change of protein levels in the full proteome of **SFN**-resistant *S. aureus* isolates compared with wild-type *S. aureus* NCTC 8325. **SFN**-resistant isolates were obtained in three independent experiments by sequential passaging in sub-MIC concentrations of **SFN** (Fig. 1e and Supplementary Fig. 6). Dark red dots represent proteins whose secretion was found to be inhibited by Arylomycin C16 (experimentally proposed SpsB substrates)[35]. Light red dots represent proteins that are predicted to have an SpsB signal peptide motif (according to UniProtKB as annotated by SignalP)[56]. Purple circles represent PGH domain-containing proteins (Pfam annotations)[55]. The proteins highlighted are fmtC (mprF, phosphatidylglycerol lysyltransferase; Q2G2M2), emp (extracellular matrix protein-binding protein emp; Q2G012), sbi (immunoglobulin-binding protein sbi; Q2FVK5), sle1 (*N*-acetylmuramoyl-L-alanine amidase sle1; Q2G0U9), spa (immunoglobulin G-binding protein A; P02976), ssaA (staphylococcal secretory antigen SsaA; Q2FV55), ssaA2 (staphylococcal secretory antigen ssaA2; Q2G2J2), arcR (HTH-type transcriptional regulator ArcR; Q2FUY1), arcA (arginine deiminase; Q2FUX7), arcC2 (carbamate kinase 2; Q7X2S2) and arcF (ornithine carbamoyltransferase; Q2FUX8). The data represent average values and the *P* values were calculated using a two-sided two-sample *t*-test; $n = 4$ independent experiments per group. **b**, Resistance towards **SFN** provokes changes in the compound-induced SpsB stimulation. SpsB activity was determined by a FRET-based peptidase activity assay using membranes of **SFN**-resistant *S. aureus* or transposon mutant NE1360 (insertion into *mprF*) as the source of endogenous SpsB (0.2 mg ml^{-1} total membrane protein concentration). The substrate cleavage rates are normalized to DMSO-treated samples. The data represent mean values ± s.d. of averaged triplicates of $n = 4$ (50 μM conditions) or $n = 3$ (rest) biologically independent experiments (individual membrane preparations) for wild-type and **SFN**-resistant isolates, and $n = 5$ independent experiments (individual measurements on different days, derived from two different membrane preparations) for NE1360. **c**, Secretome analysis of **SFN**-resistant isolates. The volcano plots show a $\log_2$-fold change of protein levels in the secretome after treatment of **SFN**-resistant *S. aureus* NCTC 8325 cells with **SFN** (1.5 μM, 0.5-fold MIC) compared with DMSO treatment. Colour coding is equivalent to that in **a**. The data represent average values and the *P* values were calculated using a two-sided two-sample *t*-test; $n = 4$ independent experiments per group.

a

PK parameter	10 mg kg^{-1} i.v.	10 mg kg^{-1} p.o.	20 mg kg^{-1} p.o.
$t_{1/2}$ (h)	11.69 ± 1.5	9.67 ± 0.2	9.37 ± 0.5
C_{max} (μg ml^{-1})	6.19 ± 3.0	1.02 ± 0.3	1.58 ± 0.2
T_{max} (h)	–	6.67 ± 2.3	5.33 ± 2.3
AUC ((μg ml^{-1})h)	33.61 ± 3.3	21.09 ± 4.0	45.09 ± 5.1
MRT (h)	10.10 ± 1.7	13.78 ± 0.5	16.71 ± 1.9
Vz/F (l kg^{-1})	5.00 ± 0.2	6.78 ± 1.3	6.07 ± 1.1
Cl/F (ml kg^{-1} h^{-1})	299.64 ± 31.0	484.77 ± 83.7	447.62 ± 53.2

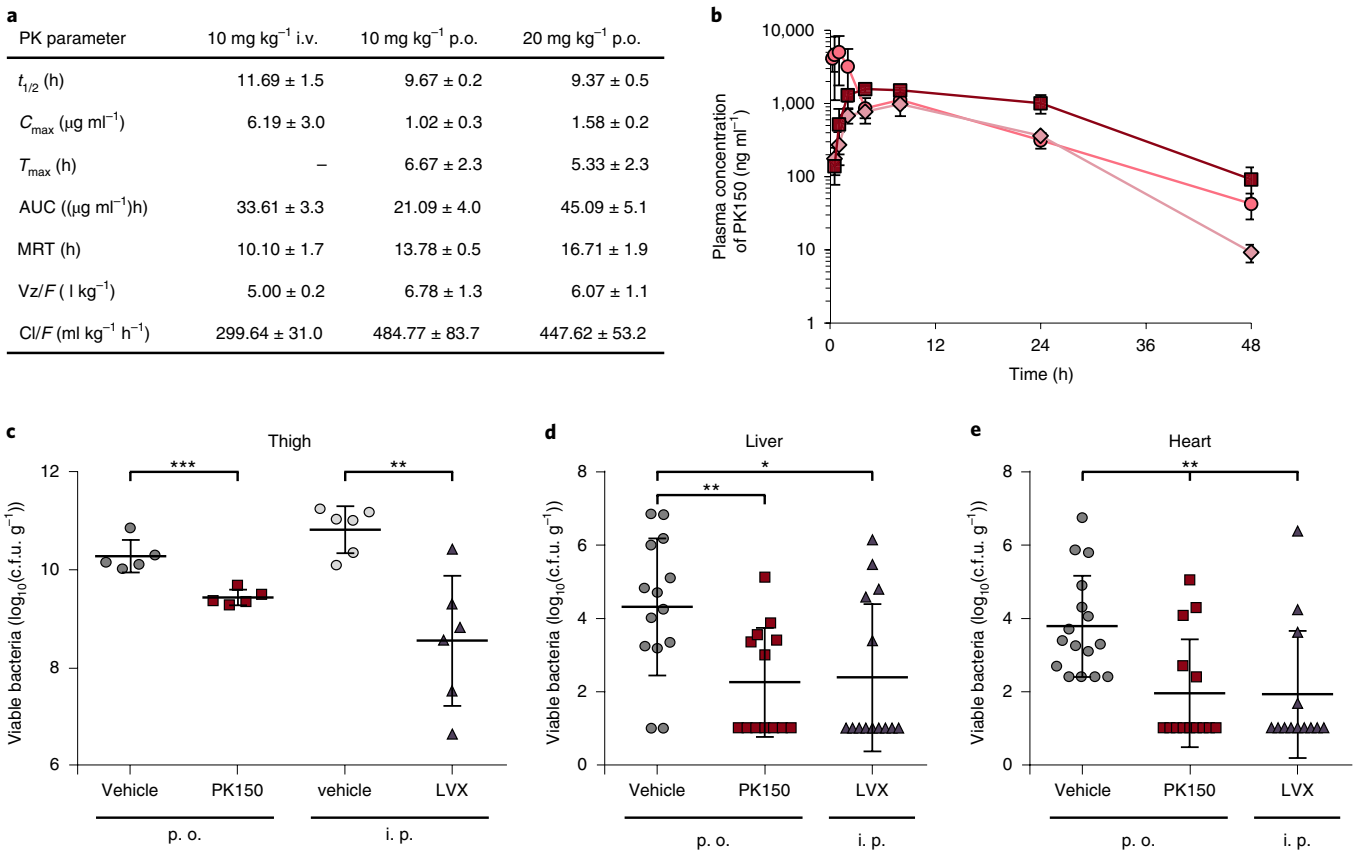

Fig. 7 | Pharmacokinetic and pharmacodynamic parameters of PK150 and in vivo efficacy. a, **PK150** pharmacokinetic parameters in murine plasma after p.o. or i.v. administration. The data represent mean ± s.d. (n = 3 per group). **b**, Pharmacokinetic analysis of **PK150** in murine plasma after p.o. or i.v. administration. Time-dependent plasma concentrations after the administration of 10 mg kg^{-1} p.o. (diamonds), 20 mg kg^{-1} p.o. (squares) or 10 mg kg^{-1} i.v. (circles) are shown. The compound levels in the plasma were determined by LC–MS/MS analysis. The data represent mean ± s.d. (n = 3 per group). **c**, Efficacy of **PK150** and LVX against *S. aureus* ATCC 33591 (MRSA) in the neutropenic murine thigh model. **PK150** (20 mg kg^{-1} p.o.) and the corresponding vehicle were administered p.o. 30 min, 4 h and 8 h after bacterial inoculation, whereas LVX (5 mg kg^{-1}) and the corresponding vehicle were administered intraperitoneally (i.p.) 2 h, 6 h and 10 h after bacterial inoculation. The data are expressed as mean ± s.d., n = 5 for **PK150** and vehicle p.o., n = 6 for LVX and vehicle i.p. ***P = 0.00093, **P = 0.0028 (two-sided Student's t-test). **d**,**e**, Efficacy of **PK150** against *S. aureus* SH1000 in a murine bloodstream infection model. Bacterial loads in the liver (**d**) and heart (**e**) of *S. aureus*-infected mice treated with **PK150** (20 mg kg^{-1} p.o. (squares)) or vehicle alone (circles) via the p.o. administration route or with LVX (triangles) via the i.p. administration route. Each symbol represents an individual mouse. Compilation data from three independent experiments are presented. Horizontal lines represent the mean ± s.d. **d**, n = 14 for vehicle and LVX, n = 13 for **PK150**. **P = 0.0040, *P = 0.014 (two-sided Student's t-test). **e**, n = 16 for vehicle, n = 14 for **PK150**, n = 13 for LVX. **P = 0.0016 (**PK150**) and P = 0.0032 (LVX, two-sided Student's t-test). $t_{1/2}$, half-life; C_{max}, maximum plasma concentration; T_{max}, time point of C_{max}; MRT, mean residence time; Vz, volume of distribution; Cl, clearance; F, bioavailability.

half-maximum inhibitory concentration (IC_{50}) values that ranged from 7 to 15 μM (Supplementary Table 4). The corresponding selectivity ratios of cytotoxicity to antibiotic activity (ratios between 23 and 52) suggest a therapeutic window for the treatment of bacterial infections in vivo. **PK150** does not cause haemolysis of red blood cells and, similarly to **SFN**, exhibits excellent plasma stability with no observable degradation after six hours of incubation (Supplementary Figs. 25 and 26).

With this promising in vitro pre-evaluation, **PK150** was subjected to pharmacokinetic studies in mice (Fig. 7a,b). No obvious signs of toxicity were observed for 10 and 20 mg kg^{-1} orally (p.o.) and for 10 mg kg^{-1} intravenously (i.v.). Higher i.v. dosing of 20 mg kg^{-1} resulted in severe toxic effects and was thus avoided for subsequent therapeutic models. Oral bioavailability was approximately 63% and the mean residence time was slightly enhanced via this administration route.

A neutropenic mouse thigh model was used to determine the pharmacodynamic efficacy of repeated **PK150** dosing (20 mg kg^{-1} p.o.) against MRSA strain ATCC 33591 (Fig. 7c). A tenfold reduction in c.f.u. g^{-1} in thighs was observed in **PK150**-treated mice in comparison with vehicle-treated mice. The same range of reduction was determined for mice treated with the positive control levofloxacin (LVX) on i.p. administration (5 mg kg^{-1}).

The in vivo efficacy of PK150 against MSSA (strain SH1000) was further demonstrated in a murine bloodstream infection model. Although no effect was observed in the kidneys (Supplementary Fig. 27), bacterial loads in the liver and heart were both significantly reduced by approximately 100-fold (Fig. 7d,e). In comparison to the marketed antibiotic LVX as the benchmark control, **PK150** exhibited not only an equal potency but also convenient dosing intervals of up to two days and good bioavailability[44,45].

Discussion

The repurposing of drugs has become an attractive strategy in the search for innovative medicine without going through enormous efforts of de novo pharmacological optimization procedures[46]. Given the drought in the discovery of new antibiotics on the one hand and the large number of about 300 bacterial proteins with

predicted essential function[47] on the other, mining bacterial proteomes with known drugs for untargeted pathways represents an attractive strategy to unravel new and resistance-free drug candidates. In our phenotypic screen of small molecule kinase inhibitors for antistaphylococcal activity, **SFN** stood out as the best antibiotic hit molecule. However, chemical proteomic profiling with its corresponding probe revealed not a single known kinase as a potential bacterial target. Moreover, in-depth SAR revealed the pyridine moiety, a hallmark of kinase inhibition[48,49], to be dispensable for antibiotic activity. Instead several other putative bacterial protein targets, foremost two essential proteins, MenG and SpsB, were identified. Of note, we cannot exclude that additional non-proteinogenous targets may exist and contribute to the overall mode of action.

MenG catalyses the final step in menaquinone biosynthesis and the disruption of MenG activity by small molecules led to antibiotic activity in other bacterial strains[28,50]. We identified MenG as one of the strongest hits in our A*f*BPP experiment with the **PK150**-derived photoprobe **3-005-P**. In accordance with this finding, **PK150** reduced menaquinone levels in living bacteria, inhibited MenG in cellular lysates and exhibited reduced antibiotic activity in the presence of exogenous menaquinone, whereas with **SFN** these effects were less pronounced. Of note, although **SFN** does not exhibit a strong effect on menaquinone biosynthesis, upregulation of the alternative arginine pathway in whole proteomes of **SFN**-resistant cells provides an independent link to alterations in the cellular energy metabolism.

Inhibition of SpsB is a challenging task as the enzyme is insensitive to classical serine protease inhibitors[51]. Besides synthetic molecules, natural products of the arylomycin family represent the most potent inhibitors[22,32]. Contrary to the well-explored inhibitory path, we discovered the first activation mechanism of SpsB. How can SpsB activation contribute to killing of bacterial cells? The analysis of bacteria treated with **PK150** or **SFN** at sub-MIC concentrations confirmed that the secretion of SpsB-dependent proteins was significantly elevated. SpsB controls a key enzymatic step that facilitates mature protein release after translocation in the membrane. Although little is known about the rate-determining step in protein secretion, studies of surface and extracellular proteomes revealed an accumulation of Sec- and SpsB-dependent proteins in the surfaceome[52–54]. Indeed, we observed a reduction of cell surface proteins prone to triggered SpsB processing on compound addition. In principle, a depot of SpsB substrates could be available on the cell surface under normal conditions and readily mobilized on enzyme stimulation to respond to external challenges. It is thus likely that, in contrast to SpsB inhibition, in which proteins are trapped in the membrane and thereby propagate cell lysis, the general dysregulation of secretion induces a similar stress to bacterial cell integrity. This is supported by the observed induction of lysis and rapid bactericidal killing of exponentially growing bacterial cells, as well as by lesions visible in electron microscopy examination. In light of the upregulation of several autolysins in the secretome, it is likely that, in line with previous literature studies, a slight imbalance of these degradative and tightly controlled enzymes could trigger autolysis[36,37]. Interestingly, we observed the downregulation of several autolysins in proteomes of **SFN**-resistant strains.

PK150's descent from a marketed drug turned out to be a beneficial property as the molecule already exhibited excellent stability and pharmacokinetic properties, which included oral bioavailability. Optimization from **SFN** to **PK150** resulted in a loss of human kinase affinity (more details in the Supplementary Discussion). Although in vitro toxicity only slightly changed, the greater antibacterial potency provided a suitable therapeutic window. **PK150** exhibits optimal stability and oral bioavailability as well as a suitable in vivo efficacy. Ongoing medicinal chemistry studies are being performed to further optimize the solubility, toxicity and spectrum of addressed bacteria to further exploit the antibiotic potential of this promising drug candidate in preclinical disease models.

Methods

The Supplementary Information gives detailed methods and protocols.

Activity-based protein profiling in *S. aureus* NCTC 8325. *S. aureus* NCTC 8325 overnight cultures were diluted 1:10 in B medium and incubated at 37 °C, 200 r.p.m. After 7 h, the bacterial cells were harvested, washed and resuspended in PBS to give a final theoretical OD_{600} of 40, then aliquoted and the photoprobe (**SFN-P**, 50 µM, or **3-005-P**, 5 µM) or DMSO (1% final total concentration) were added, followed by incubation at 25 °C, 700 r.p.m. for 45 min. For competition experiments, the cultures were first incubated with competitor **SFN** (0.5 mM) or DMSO only for 45 min before the addition of the photoprobe. After compound treatment, samples were diluted with PBS (5 ml final volume) and irradiated for 30 min with ultraviolet light (360 nm). Subsequently, the bacteria were harvested, washed and resuspended in PBS (supplemented with EDTA-free protease inhibitors) and lysed mechanically (Precellys Lysing Kit and Homogenizer). The lysate was treated with 8 µg ml^{-1} lysostaphin (37 °C, 20 min). Separation of the soluble and insoluble fractions was performed by centrifugation (21,000*g*, 4 °C, 1 h). The insoluble fraction was washed twice with PBS. Note that no separation of the soluble and insoluble fractions was done for labelling with **3-005-P**. Protein concentration was measured by bicinchoninic acid assay and samples were adjusted to equal protein amounts. For click chemistry (CuACC), the click reagents were added to each sample at the indicated final concentrations: trifunctional linker (TFL, 60 µM)[55], tris(2-carboxyethyl)phosphine (1 mM), Tris((1-benzyl-4-triazolyl)methyl)amine ligand (0.1 mM) and $CuSO_4$ (1 mM). Samples were incubated at room temperature for 1 h. After the CuACC, proteins were precipitated with ice-cold acetone (four volumes) at –20 °C overnight, washed twice with ice-cold methanol and resuspended in 0.4% (w/v) SDS in PBS. Following avidin-bead enrichment, samples were reduced with 5 mM tris(2-carboxyethyl) phosphine (1 h at 37 °C), alkylated using 10 mM iodoacetamide (30 min at 25 °C) and quenched with 10 mM dithiothreitol (30 min at 25 °C) on-bead. Proteins were predigested using LysC (2 h at 25 °C) and then digested with trypsin (16 h at 37 °C). Samples were desalted using SepPak C18 cartridges (50 mg, Waters) prior to mass spectrometry measurement. For **SFN-P**, this was accompanied by stable isotope dimethyl labelling on-column, whereas for **3-005-P**, label-free quantification (LFQ) was used. LC–MS/MS analysis was performed with an Ultimate3000 Nano-HPLC system (Thermo Fisher Scientific) coupled to an Orbitrap Fusion (for **SFN-P**, Thermo Fisher Scientific) or to a Q Exactive Plus (for **3-005-P**, Thermo Fisher Scientific). Peptide and protein identification was performed using MaxQuant[56] with Andromeda[57] as the search engine and the Uniprot database for *S. aureus* NCTC 8325. Statistical analysis was performed in Perseus[58]. Three biological replicates that consisted of three technical replicates each were analysed. Putative contaminants, reverse hits and proteins, identified by side only, were removed. For **SFN-P**, normalized protein ratios were $\log_2(x)$ transformed and filtered to contain at least one valid value within technical replicates. Ratios were *z*-score normalized within replicates and average values of the technical replicates were calculated. Mean differences in enrichment and respective *P* values were obtained by a two-sided one-sample *t*-test over the three biological replicates. For **3-005-P**, LFQ intensities were grouped into DMSO- and probe-treated condition and filtered to contain at least six valid values within at least one group. LFQ intensities were then averaged between technical replicates and $\log_2(x)$ transformed. Missing values were imputated from normal distribution and the *P* values were obtained by a two-sided two-sample *t*-test over the three biological replicates.

Supporting information gives a detailed description of the proteomic workflow.

Animal studies. The animal studies were conducted in accordance with the recommendations of the European Community (Directive 86/609/EEC, 24 November 1986). All animal procedures were performed in strict accordance with the German regulations of the Society for Laboratory Animal Science and the European Health Law of the Federation of Laboratory Animal Science Associations. Animals were excluded from further analysis if they needed to be killed according to the humane endpoints established by the ethical board. All experiments were approved by the ethical board of the Niedersächsisches Landesamt für Verbraucherschutz und Lebensmittelsicherheit (permit no. 33.9-42502-04-13/1195 and 33.19-42502-04-15/1857).

Online content

Any Nature Research reporting summaries, source data, extended data, supplementary information, acknowledgements, peer review information; details of author contributions and competing interests; and statements of data and code availability are available at https://doi.org/10.1038/s41557-019-0378-7.

Received: 10 May 2019; Accepted: 15 October 2019;
Published online: 16 December 2019

References

1. Cassini, A. et al. Attributable deaths and disability-adjusted life-years caused by infections with antibiotic-resistant bacteria in the EU and the European

Economic Area in 2015: a population-level modelling analysis. *Lancet Infect. Dis.* **19**, 56–66 (2019).
2. Tacconelli, E. et al. Discovery, research, and development of new antibiotics: the WHO priority list of antibiotic-resistant bacteria and tuberculosis. *Lancet Infect. Dis.* **18**, 318–327 (2018).
3. Tong, S. Y. C., Davis, J. S., Eichenberger, E., Holland, T. L. & Fowler, V. G. *Staphylococcus aureus* infections: epidemiology, pathophysiology, clinical manifestations, and management. *Clin. Microbiol. Rev.* **28**, 603–661 (2015).
4. Harms, A., Maisonneuve, E. & Gerdes, K. Mechanisms of bacterial persistence during stress and antibiotic exposure. *Science* **354**, aaf4268 (2016).
5. Ling, L. L. et al. A new antibiotic kills pathogens without detectable resistance. *Nature* **517**, 455–459 (2015).
6. Sass, P. et al. Antibiotic acyldepsipeptides activate ClpP peptidase to degrade the cell division protein FtsZ. *Proc. Natl Acad. Sci. USA* **108**, 17474–17479 (2011).
7. Smith, P. A. et al. Optimized arylomycins are a new class of Gram-negative antibiotics. *Nature* **561**, 189–194 (2018).
8. Kurosu, M. & Begari, E. Bacterial protein kinase inhibitors. *Drug Dev. Res* **71**, 168–187 (2010).
9. Miller, J. R. et al. A class of selective antibacterials derived from a protein kinase inhibitor pharmacophore. *Proc. Natl Acad. Sci. USA* **106**, 1737–1742 (2009).
10. Chang, H.-C. et al. In vitro and in vivo activity of a novel sorafenib derivative SC5005 against MRSA. *J. Antimicrob. Chemother.* **71**, 449–459 (2016).
11. Roberts, J. L. et al. GRP78/DNA K is a target for Nexavar/Stivarga/Votrient in the treatment of human malignancies, viral infections and bacterial diseases. *J. Cell. Physiol.* **230**, 2552–2578 (2015).
12. Pujol, E. et al. Pentafluorosulfanyl-containing triclocarban analogues with potent antimicrobial activity. *Molecules* **23**, 2853 (2018).
13. Walsh, S. E. et al. Activity and mechanisms of action of selected biocidal agents on Gram-positive and -negative bacteria. *J. Appl. Microbiol.* **94**, 240–247 (2003).
14. Conlon, B. P. et al. Activated ClpP kills persisters and eradicates a chronic biofilm infection. *Nature* **503**, 365–370 (2013).
15. Springer, M. T., Singh, V. K., Cheung, A. L., Donegan, N. P. & Chamberlain, N. R. Effect of clpP and clpC deletion on persister cell number in *Staphylococcus aureus*. *J. Med. Microbiol.* **65**, 848–857 (2016).
16. Waters, E. M., Rowe, S. E., O'Gara, J. P. & Conlon, B. P. Convergence of *Staphylococcus aureus* persister and biofilm research: can biofilms be defined as communities of adherent persister cells? *PLoS Pathog.* **12**, e1006012 (2016).
17. Hamamoto, H. et al. Lysocin E is a new antibiotic that targets menaquinone in the bacterial membrane. *Nat. Chem. Biol.* **11**, 127–133 (2015).
18. Evans, M. J. & Cravatt, B. F. Mechanism-based profiling of enzyme families. *Chem. Rev.* **106**, 3279–3301 (2006).
19. Fonović, M. & Bogyo, M. Activity-based probes as a tool for functional proteomic analysis of proteases. *Expert Rev. Proteomics* **5**, 721–730 (2008).
20. Kleiner, P., Heydenreuter, W., Stahl, M., Korotkov, V. S. & Sieber, S. A. A whole proteome inventory of background photocrosslinker binding. *Angew. Chem. Int. Ed.* **56**, 1396–1401 (2017).
21. Boersema, P. J., Raijmakers, R., Lemeer, S., Mohammed, S. & Heck, A. J. R. Multiplex peptide stable isotope dimethyl labeling for quantitative proteomics. *Nat. Protoc.* **4**, 484–494 (2009).
22. Rao, C. V. S., Waelheyns, E. D., Economou, A. & Anné, J. Antibiotic targeting of the bacterial secretory pathway. *Biochim. Biophys. Acta* **1843**, 1762–1783 (2014).
23. Cox, J. et al. Accurate proteome-wide label-free quantification by delayed normalization and maximal peptide ratio extraction, termed MaxLFQ. *Mol. Cell. Proteomics* **13**, 2513–2526 (2014).
24. Boersch, M., Rudrawar, S., Grant, G. & Zunk, M. Menaquinone biosynthesis inhibition: a review of advancements toward a new antibiotic mechanism. *RSC Adv.* **8**, 5099–5105 (2018).
25. Kurosu, M. & Begari, E. Vitamin K_2 in electron transport system: are enzymes involved in vitamin K_2 biosynthesis promising drug targets? *Molecules* **15**, 1531–1553 (2010).
26. Fey, P. D. et al. A genetic resource for rapid and comprehensive phenotype screening of nonessential *Staphylococcus aureus* genes. *mBio* **4**, e00537 (2013).
27. Craney, A., Dix, M. M., Adhikary, R., Cravatt, B. F. & Romesberg, F. E. An alternative terminal step of the general secretory pathway in *Staphylococcus aureus*. *mBio* **6**, e01178 (2015).
28. Benkovic, S. J. et al. Identification of borinic esters as inhibitors of bacterial cell growth and bacterial methyltransferases, CcrM and MenH. *J. Med. Chem.* **48**, 7468–7476 (2005).
29. Rao, C. V. S. et al. Enzymatic investigation of the *Staphylococcus aureus* type I signal peptidase SpsB—implications for the search for novel antibiotics. *FEBS J.* **276**, 3222–3234 (2009).
30. Therien, A. G. et al. Broadening the spectrum of β-lactam antibiotics through inhibition of signal peptidase type I. *Antimicrob. Agents Chemother.* **56**, 4662–4670 (2012).
31. Antes, I. DynaDock: a new molecular dynamics-based algorithm for protein–peptide docking including receptor flexibility. *Proteins* **78**, 1084–1104 (2010).
32. Craney, A. & Romesberg, F. E. The inhibition of type I bacterial signal peptidase: biological consequences and therapeutic potential. *Bioorg. Med. Chem. Lett.* **25**, 4761–4766 (2015).
33. Smith, P. A. & Romesberg, F. E. Mechanism of action of the arylomycin antibiotics and effects of signal peptidase I inhibition. *Antimicrob. Agents Chemother.* **56**, 5054–5060 (2012).
34. Walsh, S. I., Craney, A. & Romesberg, F. E. Not just an antibiotic target: exploring the role of type I signal peptidase in bacterial virulence. *Bioorg. Med. Chem.* **24**, 6370–6378 (2016).
35. Schallenberger, M. A., Niessen, S., Shao, C., Fowler, B. J. & Romesberg, F. E. Type I signal peptidase and protein secretion in *Staphylococcus aureus*. *J. Bacteriol.* **194**, 2677–2686 (2012).
36. Chao, M. C. et al. Protein complexes and proteolytic activation of the cell wall hydrolase RipA regulate septal resolution in mycobacteria. *PLoS Pathog.* **9**, e1003197 (2013).
37. Frankel, M. B., Hendrickx, A. P. A., Missiakas, D. M. & Schneewind, O. LytN, a murein hydrolase in the cross-wall compartment of *Staphylococcus aureus*, is involved in proper bacterial growth and envelope assembly. *J. Biol. Chem.* **286**, 32593–32605 (2011).
38. Pinho, M. G., Kjos, M. & Veening, J.-W. How to get (a)round: mechanisms controlling growth and division of coccoid bacteria. *Nat. Rev. Microbiol.* **11**, 601–614 (2013).
39. Makhlin, J. et al. *Staphylococcus aureus* ArcR controls expression of the arginine deiminase operon. *J. Bacteriol.* **189**, 5976–5986 (2007).
40. Ernst, C. M. & Peschel, A. Broad-spectrum antimicrobial peptide resistance by MprF-mediated aminoacylation and flipping of phospholipids. *Mol. Microbiol* **80**, 290–299 (2011).
41. Jones, T. et al. Failures in clinical treatment of *Staphylococcus aureus* infection with daptomycin are associated with alterations in surface charge, membrane phospholipid asymmetry, and drug binding. *Antimicrob. Agents Chemother.* **52**, 269–278 (2008).
42. Roy, H. Tuning the properties of the bacterial membrane with aminoacylated phosphatidylglycerol. *IUBMB Life* **61**, 940–953 (2009).
43. Médard, G. et al. Optimized chemical proteomics assay for kinase inhibitor profiling. *J. Proteome Res.* **14**, 1574–1586 (2015).
44. Fish, D. N. & Chow, A. T. The clinical pharmacokinetics of levofloxacin. *Clin. Pharmacokinet.* **32**, 101–119 (1997).
45. Scaglione, F., Mouton, J. W., Mattina, R. & Fraschini, F. Pharmacodynamics of levofloxacin and ciprofloxacin in a murine pneumonia model: peak concentration/MIC versus area under the curve/MIC ratios. *Antimicrob. Agents Chemother.* **47**, 2749–2755 (2003).
46. Nosengo, N. Can you teach old drugs new tricks? *Nature* **534**, 314–316 (2016).
47. Xu, H. H. et al. *Staphylococcus aureus* TargetArray: comprehensive differential essential gene expression as a mechanistic tool to profile antibacterials. *Antimicrob. Agents Chemother.* **54**, 3659–3670 (2010).
48. Wan, P. T. C. et al. Mechanism of activation of the RAF-ERK signaling pathway by oncogenic mutations of B-RAF. *Cell* **116**, 855–867 (2004).
49. Wu, P., Nielsen, T. E. & Clausen, M. H. FDA-approved small-molecule kinase inhibitors. *Trends Pharmacol. Sci.* **36**, 422–439 (2015).
50. Sukheja, P. et al. A novel small-molecule inhibitor of the *Mycobacterium tuberculosis* demethylmenaquinone methyltransferase MenG is bactericidal to both growing and nutritionally deprived persister cells. *mBio* **8**, e02022 (2017).
51. Paetzel, M., Dalbey, R. E. & Strynadka, N. C. J. Crystal structure of a bacterial signal peptidase in complex with a β-lactam inhibitor. *Nature* **396**, 186–190 (1998).
52. Dreisbach, A., van Dijl, J. M. & Buist, G. The cell surface proteome of *Staphylococcus aureus*. *Proteomics* **11**, 3154–3168 (2011).
53. Gatlin, C. L. et al. Proteomic profiling of cell envelope-associated proteins from *Staphylococcus aureus*. *Proteomics* **6**, 1530–1549 (2006).
54. Hempel, K. et al. Quantitative cell surface proteome profiling for SigB-dependent protein expression in the human pathogen *Staphylococcus aureus* via biotinylation approach. *J. Proteome Res.* **9**, 1579–1590 (2010).
55. Eirich, J. et al. Pretubulysin derived probes as novel tools for monitoring the microtubule network via activity-based protein profiling and fluorescence microscopy. *Mol. BioSyst.* **8**, 2067–2075 (2012).
56. Cox, J. & Mann, M. MaxQuant enables high peptide identification rates, individualized p.p.b.-range mass accuracies and proteome-wide protein quantification. *Nat. Biotechnol.* **26**, 1367–1372 (2008).
57. Cox, J. et al. Andromeda: a peptide search engine integrated into the MaxQuant environment. *J. Proteome Res.* **10**, 1794–1805 (2011).

58. Vizcaíno, J. A. et al. 2016 update of the PRIDE database and its related tools. *Nucleic Acids Res.* **44**, 11033–11033 (2016).
59. Tyanova, S. et al. The Perseus computational platform for comprehensive analysis of (prote)omics data. *Nat. Methods* **13**, 731–740 (2016).
60. Finn, R. D. et al. The Pfam protein families database: towards a more sustainable future. *Nucleic Acids Res.* **44**, D279–D285 (2016).
61. Nielsen, H. Predicting secretory proteins with SignalP. *Methods Mol. Biol.* **1611**, 59–73 (2017).

Reporting summary. Further information on research design is available in the Nature Research Reporting Summary linked to this article.

Data availability

The mass spectrometry proteomics data have been deposited at the ProteomeXchange Consortium via the PRIDE[59] partner repository with the dataset identifier PXD012946. Whole-genome sequencing data and metadata are available on the SRA repository under the Bioproject number PRJNA525411. Bacterial strains and plasmids used in this work are readily available from the authors, or can be purchased commercially as stated in the Supplementary Information.

Code availability

All computer code used is either publicly available software, described in prior publications[31] or available from the authors upon request. For details on the versions and parameters used, please refer to the respective sections in the Supplementary Information.

Acknowledgements

We thank the Network on Antimicrobial Resistance in *Staphylococcus aureus* (NARSA) for the supply of the Nebraska Transposon Mutant Library (NTML). Furthermore, we thank S. Grond for providing arylomycin and F. Romesberg for providing *S. aureus* N315 ARC0001ΔSpsB. We also thank S. Miami and E. Rubin for determining the antimicrobial activities against *M. tuberculosis*. We thank A. Klaschwitz, F. Kortmann, S. Hifinger and C. Lierse von Gostomski for the scintillation measurement of radioactively labelled menaquinone. S.A.S. was funded by the Center for Integrated Protein Science Munich (CIPSM), Deutsche Forschungsgemeinschaft SFB1035 and European Research Council (ERC) and the European Union's Horizon 2020 research and innovation programme (grant agreement no. 725085, CHEMMINE, ERC consolidator grant). E.K. was supported by a doctoral fellowship of the Fonds der Chemischen Industrie. R.M. was supported by a doctoral fellowship of the Boehringer Ingelheim Fonds. K.R. was supported by the German Centre for Infection Research (DZIF) (TTU 09.710). I.A. acknowledges funding by Deutsche Forschungsgemeinschaft SFB1035. W.M.W. was funded by the National Science Foundation (CHE-1454116) and the National Institute of General Medical Sciences (R35 GM119426). M.C.J. acknowledges a National Science Foundation predoctoral grant (DGE-1144462). S.M.H. acknowledges financial support by a Liebig fellowship of the Fonds der Chemischen Industrie. M.W.H., C.F. and F.A.M.M. were funded by the Federal Ministry for Education and Research (BMBF) under the framework programme 'VIP+'—project 'aBacter'. We thank D. Mostert for excellent experimental support, M. Wolff, K. Bäuml, K. Gliesche, L. Nguyen and J. Schreiber for excellent technical support and M. Stahl for critical comments on the manuscript.

Author contributions

P.L., E.K., R.M. and S.A.S. designed the experiments, interpreted the results and wrote the manuscript with input from all the authors. P.L. synthesized the library compounds and probes and performed SAR studies. V.S.K. assisted in the chemical synthesis of the A*f*BPP probes. E.K. and P.L. performed gel- and MS-based labelling and analysis of the MS data, as well as SpsB target deconvolution and validation experiments. E.K. analysed mass spectrometry-based data and conducted bioinformatics analyses. R.M. performed target identification, MS data analysis and validation experiments in the context of the menaquinone biosynthesis pathway and assisted in further validation experiments. E.K., P.L. and S.M.H. performed the bacterial resistance development studies. E.K. carried out persister assays and time-kill assays. M.W.H., C.F. and F.A.M.M. performed time-kill assays as well as biofilm and persister studies. M.C.J. and W.M.W. helped in the biofilm studies. J.L. performed microbiological studies in mycobacteria. D.C.-M. and D.H.P. conducted the whole-genome sequencing of resistant bacterial isolates and analysed the related data. I.U. and I.A. performed molecular docking and dynamic studies and interpreted the related data. K.R. and M.Rohde performed electron microscopy studies and analysed the related data. M.Reinecke and B.K. performed kinobead pull-down experiments and analysed the related data. K.R. and E.M. performed animal studies and analysed the related data.

Competing interests

P.L., E.K. and S.A.S. are co-inventors on a European patent (EP 16 171 906.7) that covers the structure of **PK150**. All the other authors declare no competing interests.

Additional information

Supplementary information is available for this paper at https://doi.org/10.1038/s41557-019-0378-7.

Correspondence and requests for materials should be addressed to S.A.S.

Reprints and permissions information is available at www.nature.com/reprints.

nature research

Corresponding author(s): Stephan A. Sieber

Last updated by author(s): Sep 6, 2019

Reporting Summary

Nature Research wishes to improve the reproducibility of the work that we publish. This form provides structure for consistency and transparency in reporting. For further information on Nature Research policies, see Authors & Referees and the Editorial Policy Checklist.

Statistics

For all statistical analyses, confirm that the following items are present in the figure legend, table legend, main text, or Methods section.

n/a	Confirmed
☐	☒ The exact sample size (*n*) for each experimental group/condition, given as a discrete number and unit of measurement
☐	☒ A statement on whether measurements were taken from distinct samples or whether the same sample was measured repeatedly
☐	☒ The statistical test(s) used AND whether they are one- or two-sided *Only common tests should be described solely by name; describe more complex techniques in the Methods section.*
☒	☐ A description of all covariates tested
☐	☒ A description of any assumptions or corrections, such as tests of normality and adjustment for multiple comparisons
☐	☒ A full description of the statistical parameters including central tendency (e.g. means) or other basic estimates (e.g. regression coefficient) AND variation (e.g. standard deviation) or associated estimates of uncertainty (e.g. confidence intervals)
☐	☒ For null hypothesis testing, the test statistic (e.g. *F*, *t*, *r*) with confidence intervals, effect sizes, degrees of freedom and *P* value noted *Give P values as exact values whenever suitable.*
☒	☐ For Bayesian analysis, information on the choice of priors and Markov chain Monte Carlo settings
☒	☐ For hierarchical and complex designs, identification of the appropriate level for tests and full reporting of outcomes
☒	☐ Estimates of effect sizes (e.g. Cohen's *d*, Pearson's *r*), indicating how they were calculated

Our web collection on statistics for biologists contains articles on many of the points above.

Software and code

Policy information about availability of computer code

Data collection	Chromeleon was used for aquisition of MS data. Optical absoprtions and fluorescence measurements were recorded with Tecan i-control (v. 3.9.1.0). Gel images were recorded with Image Reader LAS-4000 (v. 2.1, Fujifilm). Dynamic light scattering was recorded with Dynamics 7.8.0.26 (Wyatt Technology). Electron microscopy images were recorded with Zeiss SEMSmart (v. 5.05, for FESEM images) and iTEM software (build 1210, 05.10.2007, for TEM images), and contrast and brightness were adjusted with Adobe Photoshop CS5. Scintillation counting of radioactive tritium was recorded with QuantaSmart (v. 2.03, PerkinElmer).
Data analysis	Amber15, Gaussian09, DynaCell (v. 1.0) and an in-house python script (available upon request) were used for molecular docking and dynamics simulations. MaxQuant (v. 1.5.1.2; 1.5.3.30; 1.6.0.1 or 1.6.2.10) was used for analysis of MS raw data and Perseus (v. 1.5.1.6; 1.5.3.2; 1.6.0.0 or 1.6.2.2) for subsequent statistical analysis. MS data regarding MenG assays and plasma stability were analysed using XCalibur software (v. 2.1.0, Thermo Fisher Scientific). Trimmomatic (v. 0.38), Samtools (v. 1.9), Bowtie2 (v. 2.3.4.1), BWA-SW (v. 0.7.17), Freebayes (v. 1.2.0-4), vcffilter (v. 1.0.0) and snpEff (v. 4.3t) were used for bioinformatic analysis of whole genome sequencing. GraphPad Prism was used for statistical tests regarding persister cell assays, MBEC determination and ClpP peptidase assays (v. 6.05), as well as cytotoxicity data, plasma stability, and animal experiments (v. 5.03). Origin (v. 9.1G) was used for processing data from enzymatic activity assays. Pharmacokinetic data were analyzed using MultiQuant 3.0 software (AB Sciex) and pharmacokinetic parameters were determined using a non-compartmental analysis with PKSolver. Standard deviations and Fisher's exact test were performed with Microsoft Excel. For further details, please refer to the Supplementary Information.

For manuscripts utilizing custom algorithms or software that are central to the research but not yet described in published literature, software must be made available to editors/reviewers. We strongly encourage code deposition in a community repository (e.g. GitHub). See the Nature Research guidelines for submitting code & software for further information.

Data

Policy information about availability of data

All manuscripts must include a data availability statement. This statement should provide the following information, where applicable:

- Accession codes, unique identifiers, or web links for publicly available datasets
- A list of figures that have associated raw data
- A description of any restrictions on data availability

The mass spectrometry proteomics data have been deposited to the ProteomeXchange Consortium via the PRIDE partner repository with the dataset identifier PXD012946.
Whole Genome Sequencing data and metadata are available on the SRA repository under the Bioproject number PRJNA525411.

Field-specific reporting

Please select the one below that is the best fit for your research. If you are not sure, read the appropriate sections before making your selection.

☒ Life sciences ☐ Behavioural & social sciences ☐ Ecological, evolutionary & environmental sciences

For a reference copy of the document with all sections, see nature.com/documents/nr-reporting-summary-flat.pdf

Life sciences study design

All studies must disclose on these points even when the disclosure is negative.

Sample size	Statistical predetermination of sample size was not done. For all experiments with bacterial samples and in vitro assays, at least three independent biological replicates were performed to ensure reproducibility of the findings. For in vivo efficacy studies in mice, sample size was n=3 per group for pharmacokinetic analysis, n=5-6 for the neutropenic thigh model, and n=13-16 for the bloodstream infection model. These numbers are based on previous experience and, for the case of animal experiments, represent a compromise between statistical robustness of the data and the ethical limitations associated with the use of live animals.
Data exclusions	No data were excluded from the study.
Replication	All experiments were repeated independently to ensure reproducibility of the data. Numbers of replications for each experiment are stated in the respective figure legend and all attempts of replication were successful.
Randomization	Randomization was not possible for the experiments described herein and was thus not relevant for this study.
Blinding	Blinding was not possible for the experiments described herein and was thus not relevant for this study.

Reporting for specific materials, systems and methods

We require information from authors about some types of materials, experimental systems and methods used in many studies. Here, indicate whether each material, system or method listed is relevant to your study. If you are not sure if a list item applies to your research, read the appropriate section before selecting a response.

Materials & experimental systems

n/a	Involved in the study
☒	☐ Antibodies
☐	☒ Eukaryotic cell lines
☒	☐ Palaeontology
☐	☒ Animals and other organisms
☒	☐ Human research participants
☒	☐ Clinical data

Methods

n/a	Involved in the study
☒	☐ ChIP-seq
☒	☐ Flow cytometry
☒	☐ MRI-based neuroimaging

Eukaryotic cell lines

Policy information about cell lines

Cell line source(s)	All cell lines used in this study (K-562, Colo 205, SK-N-BE(2), MV-4-11, A549, NIH/3T3, HeLa and HepG2) are commonly used cell lines that were available by in-house stocks.
Authentication	Cell lines were not authenticated prior to use.
Mycoplasma contamination	Cell lines were tested negative for mycoplasma contamination.

Commonly misidentified lines (See ICLAC register)	No commonly misidentified cell lines were used.

Animals and other organisms

Policy information about studies involving animals; ARRIVE guidelines recommended for reporting animal research

Laboratory animals	Outbred male CD-1 mice, 4 weeks old, were used for pharmacokinetic and pharmacodynamic analyses. Pathogen-free 9-week old female C57BL/6J mice were used for efficacy experiments.
Wild animals	The study did not involve wild animals.
Field-collected samples	The study did not involve field-collected samples.
Ethics oversight	All experiments were approved by the ethical board of the Niedersächsisches Landesamt für Verbraucherschutz und Lebensmittelsicherheit, Oldenburg, Germany (LAVES; permit No. 33.9-42502-04-13/1195 and 33.19-42502-04-15/1857).

Note that full information on the approval of the study protocol must also be provided in the manuscript.